CONTRACT REPORT ARBRL-CR-00491

NUMERICAL SIMULATION OF LAMINAR, INCOMPRESSIBLE FLOW WITHIN LIQUID FILLED SHELLS

Prepared by

Rockwell International Corp.
Science Center
1049, Camino Dos Rios
Thousand Oaks, CA 91360

November 1982

US ARMY ARMAMENT RESEARCH AND DEVELOPMENT COMMAND
BALLISTIC RESEARCH LABORATORY
ABERDEEN PROVING GROUND, MARYLAND

Destroy this report when it is no longer needed.
Do not return it to the originator.

Secondary distribution of this report is prohibited.

Additional copies of this report may be obtained from the National Technical Information Service, U. S. Department of Commerce, Springfield, Virginia 22161.

The findings in this report are not to be construed as an official Department of the Army position, unless so designated by other authorized documents.

The use of trade names or manufacturers' names in this report does not constitute indorsement of any commercial product.

Unclassified

SECURITY CLASSIFICATION OF THIS PAGE (When Data Entered)

REPORT DOCUMENTATION PAGE		READ INSTRUCTIONS BEFORE COMPLETING FORM
1. REPORT NUMBER Contractor Report ARBRL-CR-00491	2. GOVT ACCESSION NO.	3. RECIPIENT'S CATALOG NUMBER
4. TITLE (and Subtitle) Numerical Simulation of Laminar, Incompressible Flow Within Liquid Filled Shells		5. TYPE OF REPORT & PERIOD COVERED Final Report Draft 09/29/80 - 10/30/81
		6. PERFORMING ORG. REPORT NUMBER SC5284.2FRD
7. AUTHOR(s) Sukumar R. Chakravarthy		8. CONTRACT OR GRANT NUMBER(s) DAAK11-80-C-0101
9. PERFORMING ORGANIZATION NAME AND ADDRESS Rockwell International Corp. Science Center 1049, Camino Dos Rios, Thousand Oaks, CA 91360		10. PROGRAM ELEMENT, PROJECT, TASK AREA & WORK UNIT NUMBERS
11. CONTROLLING OFFICE NAME AND ADDRESS US Army Armament Research & Development Command US Army Ballistic Research Laboratory (DRDAR-BL) Aberdeen Proving Ground, MD 21005		12. REPORT DATE November 1982 13. NUMBER OF PAGES 65
14. MONITORING AGENCY NAME & ADDRESS(if different from Controlling Office)		15. SECURITY CLASS. (of this report) Unclassified 15a. DECLASSIFICATION/DOWNGRADING SCHEDULE

16. DISTRIBUTION STATEMENT (of this Report)

Approved for public release; Distribution Unlimited.

17. DISTRIBUTION STATEMENT (of the abstract entered in Block 20, if different from Report)

18. SUPPLEMENTARY NOTES

19. KEY WORDS (Continue on reverse side if necessary and identify by block number)

Liquid filled spinning shells, numerical simulation, laminar flow, implicit finite difference scheme, axisymmetric spin-up, primitive variable formulation.

20. ABSTRACT (Continue on reverse side if necessary and identify by block number)

A numerical simulation capability has been developed for the analysis of fluid flow in liquid-filled projectiles. The unsteady, compressible Navier-Stokes equations for laminar flow are solved for the primitive variables without recourse to linearization or simplification of the equations of motion. The finite difference approximations to the governing equations are by choice either of first or second order time accuracy, second order spatial accuracy in the axial and radial directions, and fourth order spatial accuracy in the

DD FORM 1 JAN 73 1473

Unclassified

SECURITY CLASSIFICATION OF THIS PAGE (When Data Entered)

azimuthal direction. The method allows imposition of arbitrary body motions including spin and precession and the corresponding boundary conditions are easily and directly prescribed. The finite difference equations are solved using an implicit, approximate factorization procedure that permits the choice of reasonably large time steps and avoids limitations based on the magnitude of Reynolds number. Thus, the numerical simulations methodology considered provides a complete, accurate and flexible framework for the computational analysis of fluid behavior in liquid-filled projectiles.

In the current effort, two computer programs have been developed. The cartesian velocity components and pressure are the dependent variables in the first along with a cartesian base coordinate system. This code retains the desired features of arbitrary geometry and body motion. The second computer program is cast with cylindrical velocity components in cylindrical coordinates and is currently (but not inherently) limited to a cylindrical geometry. Both these programs are applicable to three-dimensional flow and both codes can be flagged to compute axisymmetric flow efficiently by avoiding calculations involving the extra coordinate. This axisymmetric option has been extensively exercised and the results compare favorably with other known numerical results. The fully three-dimensional codes have been exercised for fewer cases but enough to validate their accurate applicability.

While it was only required that either a properly formulated cartesian variable or a cylindrical variable code be constructed that can efficiently treat axisymmetric cases, both approaches have been executed in the present effort. The cartesian variable computer program solved the governing equations in conservation form while the cylindrical variable formulation used the non-conservation form and consequently somewhat different discretizations were employed in the two codes as an exercise. The cylindrical variable formulation gave better results, but the precise reason for the improvement is inconclusive yet.

TABLE OF CONTENTS

		Page
	LIST OF ILLUSTRATIONS	5
1.	SUMMARY	7
2.	INTRODUCTION	9
	BACKGROUND	9
	OBJECTIVES AND TASKS	10
	REPORT LAYOUT	12
3.	GOVERNING EQUATIONS IN CARTESIAN VARIABLES	13
	BOUNDARY CONDITIONS	20
	SUBTRACTING OUT AXISYMMETRIC VARIATION	20
4.	NUMERICAL METHOD FOR CARTESIAN VARIABLE FORMULATION	23
	SATISFYING THE CONTINUITY EQUATION	25
5.	RESULTS FOR AXISYMMETRIC SPIN-UP USING CARTESIAN VARIABLE FORMULATION	26
	GRID CLUSTERING	26
	EVOLUTION OF SPIN-UP FLOW	27
	COMPARISON WITH RESULTS FROM KITCHENS' CODE	38
6.	CYLINDRICAL VARIABLE FORMULATION	44
	RESULTS	45
7.	THREE-DIMENSIONAL RESULTS	55
8.	CONCLUDING REMARKS	57
9.	REFERENCES	58
	DISTRIBUTION LIST	59

LIST OF ILLUSTRATIONS

Figure		Page(s)
1.	Sketch of interior flow domain with coordinate definition.....	16
2.	Computational grid for Reynolds number of 10,000.....	28
3.	In-plane velocity field plots for Reynolds number 10,000.....	29-30
4.	Azimuthal velocity plots for Reynolds number 10,000.....	32
5.	Streamline contour plots for Reynolds number 10,000.....	33-34
6.	Computational grid for Reynolds number 1,000.....	35
7.	In-plane velocity field plots for Reynolds number 1,000.....	36
8.	Azimuthal velocity plots for Reynolds number 1,000.....	37
9.	Streamline contours at Time = 62.5 for Reynolds number 1,000...	37
10.	Comparison of azimuthal velocity profiles for Reynolds number 10,000 and Time = 62.5.....	39-40
11.	Time history of azimuthal velocity at axial location of 1.0 and radial location of 0.9.....	41
12.	Comparison of azimuthal velocity profiles for Reynolds number 1,000 at Time = 62.5.....	42
13.	Comparison of azimuthal velocity profiles for Reynolds number 1,000 at Time = 125.0.....	43
14.	Comparison of azimuthal velocity profiles for Reynolds number 1,000 at Time = 62.5.....	46
15.	Comparison of azimuthal velocity profiles for Reynolds number 1,000 at Time = 125.0.....	47
16.	Comparison of azimuthal velocity profiles for Reynolds number 10,000 at Time = 62.5.....	48
17.	Comparison of azimuthal velocity profiles for Reynolds number 10,000 at Time = 125.0.....	49
18.	Comparison of azimuthal velocity profiles for Reynolds number 10,000 at Time = 187.5.....	50
19.	Effect of the parameter β shown for Reynolds number 10,000 at Time = 62.5.....	51

LIST OF ILLUSTRATIONS (Continued)

Figure		Page(s)
20.	Effect of time accuracy.....	52
21a.	Computational grid for Reynolds number 1,000,000.....	54
21b.	Azimuthal velocity profiles for Reynolds number 1,000,000.....	54

1. SUMMARY

A numerical simulation capability has been developed for the analysis of fluid flow in liquid-filled projectiles. The unsteady, compressible Navier-Stokes equations for laminar flow are solved for the primitive variables without recourse to linearization or simplification of the equations of motion. The finite difference approximations to the governing equations are by choice either of first or second order time accuracy, second order spatial accuracy in the axial and radial directions, and fourth order accuracy in the azimuthal direction. The method allows imposition of arbitrary body motions including spin and precession and the corresponding boundary conditions are easily and directly prescribed. The finite difference equations are solved using an implicit, approximate factorization procedure that permits the choice of reasonably large time steps and avoids limitations based on the magnitude of Reynolds number. Thus, the numerical simulation methodology considered provides a complete, accurate and flexible framework for the computational analysis of fluid behavior in liquid-filled projectiles.

In the current effort, two computer programs have been developed. The cartesian velocity components and pressure are the dependent variables in the first along with a cartesian base coordinate system. This code retains the desired features of arbitrary geometry and body motion. The second computer program is cast with cylindrical velocity components in cylindrical coordinates and is currently (but not inherently) limited to a cylindrical geometry. Both these programs are applicable to three-dimensional flow and both codes can be flagged to compute axisymmetric flow efficiently by avoiding calculations involving the extra coordinate. This axisymmetric option has been extensively exercised and the results compare favorably with other known numerical results. The fully three-dimensional codes have been exercised for fewer cases but enough to validate their accurate applicability.

While it was only required that either a properly formulated cartesian variable or a cylindrical variable code be constructed that can efficiently treat axisymmetric cases, both approaches have been executed in the present effort. The cartesian variable computer program solved the governing equations in conservation form while the cylindrical variable formulation used the non-conservation form and consequently somewhat different discretizations were employed in the two codes as an exercise. The cylindrical variable formulation gave better results, but the precise reason for the improvement is inconclusive yet.

2. INTRODUCTION

BACKGROUND

The Army is currently developing liquid payloads for spin-stabilized projectiles. A liquid filler can destabilize the flight of an aeroballistically well designed shell. The instability mechanism is a resonance between the coning frequency of the projectile and a natural vibration frequency of the spinning liquid. Only simplified models have been used in the past to study this liquid-induced, projectile instability. These include linear models and axisymmetric (independent of circumferential or azimuthal position within the fluid) finite-difference solutions to the governing equations, the Navier-Stokes equations[1,2,3]. The linear models consist of closed form analytic solutions and/or numerical solutions. The primary deficiency with the available models is that the projectile yaw must be quite small. In fact, experiments to verify these modes indicate serious nonlinear effects at yaw amplitudes well below those common to projectiles[4]. Hence, large yaw effects must be incorporated into the modeling capabilities. Also, many of the linear models do not properly treat the boundary conditions at the liquid/solid interfaces. Corrections are required within these models, but the corrections are only valid for high Reynolds numbers. The axisymmetric Navier-Stokes code cannot model the three-dimensional disturbances within the liquid produced by the yawing motion or the three-dimensional response of the liquid. The natural frequencies of the liquid are truly three-dimensional oscillations and most flow problems cannot be treated by an axisymmetric code. A full three-dimensional solution to the Navier-Stokes equations is required. Viscous effects must be maintained properly in all coordinate directions to properly model the rotating fluid. The code must also have a high Reynolds number capability. This requires the use of a computational algorithm which is more complex than a standard finite difference solution.

This report describes the development and testing of a Navier-Stokes solver that fits the bill. The basic method was first presented by Steger and Kutler[5] as an implicit finite-difference procedure to solve the imcompressible Navier-Stokes equations used to model aircraft vortex wake flows of external aerodynamics. This code was modified extensively by Steger[6] in order to be used for the internal fluid mechanics within liquid filled shells. These changes were made to enable the computer code to accept arbitrary body motion and quite general body geometry, to minimize computer storage space, and to account for internal boundary conditions. While this code was verified to be stable for spin-up and spin-down for cylindrical geometries and showed correct flow field structure and development, it was not directly compared with other theories. Also, the computer program required too much computational time to pursue detailed spin-up calculations; having been built for arbitrary body motion and shape, it was not efficient for axisymmetric spin-up. It was thus logical to start from this computer code, make the necessary modifications to make it more efficient for axisymmetric flows and subject the method to thorough testing.

OBJECTIVES AND TASKS

Towards the overall objective of developing a numerical simulation capability for liquid-filled projectiles that is complete, accurate and flexible, this effort concentrated on modifying an existing finite difference method which potentially could meet the requirements and checking it thoroughly against known analytic and numerical solutions for simple cases. The method was also to be tested for limitations and cost for a few fully three-dimensional cases. These goals were broken up into the following tasks:

1) An existing computer code for three-dimensional incompressible flow was to be modified to produce improved efficiency and accuracy.

(This code was developed under Scientific Services Program Contract No. DAAG29-76-D-0100, but it was only superficially checked for accuracy and operational capabilities) The existing code was formulated using cartesian velocity components. These velocities are not convenient for a spinning projectile where the initial flow is axisymmetric. In order to improve the computational efficiency, the code was to be recast in cylindrical coordinates or the axisymmetric variation was to be subtracted out.

2) The code was also to be set up so that it can easily be executed in an axisymmetric mode. This capability would be necessary to evaluate questions of numerical accuracy and efficiency and to establish Reynolds number limits.

3) The code was to be structured so that the numerical scheme was of either first or second order time accuracy. Solutions of second order accuracy would allow increased efficiency by using larger time steps, but they are normally prone to more numerical instabilities. The advantages and disadvantages of larger time steps versus numerical instabilities were to be investigated for rotating fluid flow problems.

4) Solutions from the axisymmetric version of the code were to be compared to other known numerical results.

5) Run times for the three-dimensional and axisymmetric versions of the code were to be compared.

6) The axisymmetric version was to be exercised to define the limitations of the code for projectile spin rate and Reynolds number.

7) Similar to task 6 but for fewer cases, spin rate and Reynolds number limitations were to be investigated for the three-dimensional code option.

REPORT LAYOUT

The rest of this report addresses these tasks, how they were accomplished and the results of the study. Section 3 covers the governing equations with cartesian velocity components as the dependent variables. The numerical method for this formulation is described in Section 4. Results for axisymmetric spinning flow obtained using the above formulations is given in Section 5. The cylindrical variable formulation and results are shown in Section 6. The treatment in this chapter is brief in as much as the primary thrust of this effort was to check out the cartesian variable formulation. Three-dimensional results are covered in Section 7 followed by concluding remarks and a list of references in Sections 8 and 9.

3. GOVERNING EQUATIONS IN CARTESIAN VARIABLES

The motion of a liquid fluid within a container is governed by the incompressible Navier-Stokes equations.

Momentum equations

$$\partial_t \vec{q} + \partial_x(\vec{e} - \vec{e}_v) + \partial_y(\vec{f} - \vec{f}_v) + \partial_z(\vec{g} - \vec{g}_v) = 0 \tag{1a}$$

Continuity equation

$$\partial_x u + \partial_y v + \partial_z w = 0 \tag{1b}$$

where

$$\vec{q} = \begin{bmatrix} u \\ v \\ w \end{bmatrix}, \quad \vec{e} = \begin{bmatrix} u^2+p \\ uv \\ uw \end{bmatrix}, \quad \vec{f} = \begin{bmatrix} vu \\ v^2+p \\ vw \end{bmatrix}, \quad \vec{g} = \begin{bmatrix} wu \\ wv \\ w^2+p \end{bmatrix}$$

velocity components — inviscid flux terms

$$\vec{e}_v = \nu \begin{bmatrix} \partial_x u \\ \partial_x v \\ \partial_x w \end{bmatrix}, \quad \vec{f}_v = \nu \begin{bmatrix} \partial_y u \\ \partial_y v \\ \partial_y w \end{bmatrix}, \quad \vec{g}_v = \nu \begin{bmatrix} \partial_z u \\ \partial_z v \\ \partial_z w \end{bmatrix}$$

viscous terms

x, y, z -- cartesian coordinate directions, t -- time
u, v, w -- cartesian velocity components , p -- pressure
ν -- coefficient of viscosity

The continuity equation has no time derivative. To facilitate construction of an implicit , approximately factored numerical method, the continuity equation is modified to be

$$\partial_t p + \beta(\partial_x u + \partial_y v + \partial_z w) = \partial_t p^* \qquad (1c)$$

The quantities β, p^* and the numerical algorithm will be chosen to let

$$\partial_x u + \partial_y v + \partial_z w \rightarrow 0$$

(see next Section). Equations (1a) and (1c) may now be combined to yield

$$\partial_t \vec{D} + \partial_x(\vec{E}-\vec{E}_v) + \partial_y(\vec{F}-\vec{F}_v) + \partial_z(\vec{G}-\vec{G}_v) = (\partial_t p^*, 0, 0, 0)^{\text{Transpose}}$$

$$\vec{D} = \begin{bmatrix} p \\ --- \\ \vec{q} \end{bmatrix}, \quad \vec{E} = \begin{bmatrix} \beta u \\ ---- \\ \vec{e} \end{bmatrix}, \quad \vec{F} = \begin{bmatrix} \beta v \\ ---- \\ \vec{f} \end{bmatrix}, \quad \vec{G} = \begin{bmatrix} \beta w \\ ---- \\ \vec{g} \end{bmatrix} \qquad (2)$$

$$\vec{E}_v = \begin{bmatrix} 0 \\ ---- \\ \vec{e}_v \end{bmatrix}, \quad \vec{F}_v = \begin{bmatrix} 0 \\ ---- \\ \vec{f}_v \end{bmatrix}, \quad \vec{G}_v = \begin{bmatrix} 0 \\ ---- \\ \vec{g}_v \end{bmatrix}$$

In the above, the subscript v was used to denote viscous terms. But for this and other subscripts that will be clearly pointed out, the subscript notation will be used interchangeably with the derivative operator notation ∂_x, etc., to denote derivatives. Thus, $\partial_x f = f_x$.

In order to permit arbitrary body motion and shape, new independent variables (but not dependent variables) are introduced.

$$\begin{aligned} \tau &= t \\ \xi &= \xi(x,t) \\ \eta &= \eta(x,y,z,t) \\ \zeta &= \zeta(x,y,z,t) \end{aligned} \tag{3}$$

These coordinates are defined in Fig. 1. By restricting ξ to be a function of only x and t, computer storage is minimized and the computation of metrics is simplfied. Yet, little generality is lost. Using Eqs. (3), the transformed equations become

$$\partial_\tau \hat{D} + \partial_\xi(\hat{E}-\hat{E}_v) + \partial_\eta(\hat{F}-\hat{F}_v) + \partial_\zeta(\hat{G}-\hat{G}_v) = J^{-1}(\partial_t p^*,0,0,0)^{\text{Transpose}} \tag{4a}$$

where

$$\begin{aligned} \hat{D} &= \vec{D}/J \\ \hat{E} &= (\xi_t\vec{D} + \xi_x\vec{E} \qquad\qquad)/J \\ \hat{F} &= (\eta_t\vec{D} + \eta_x\vec{E} + \eta_y\vec{F} + \eta_z\vec{G})/J \\ \hat{G} &= (\zeta_t\vec{D} + \zeta_x\vec{E} + \zeta_y\vec{F} + \zeta_z\vec{G})/J \\ \hat{E}_v &= (\xi_x\vec{E}_v \qquad\qquad)/J \\ \hat{F}_v &= (\eta_x\vec{E}_v + \eta_y\vec{F}_v + \eta_z\vec{G}_v)/J \\ \hat{G}_v &= (\zeta_x\vec{E}_v + \zeta_y\vec{F}_v + \zeta_z\vec{G}_v)/J \end{aligned} \tag{4b}$$

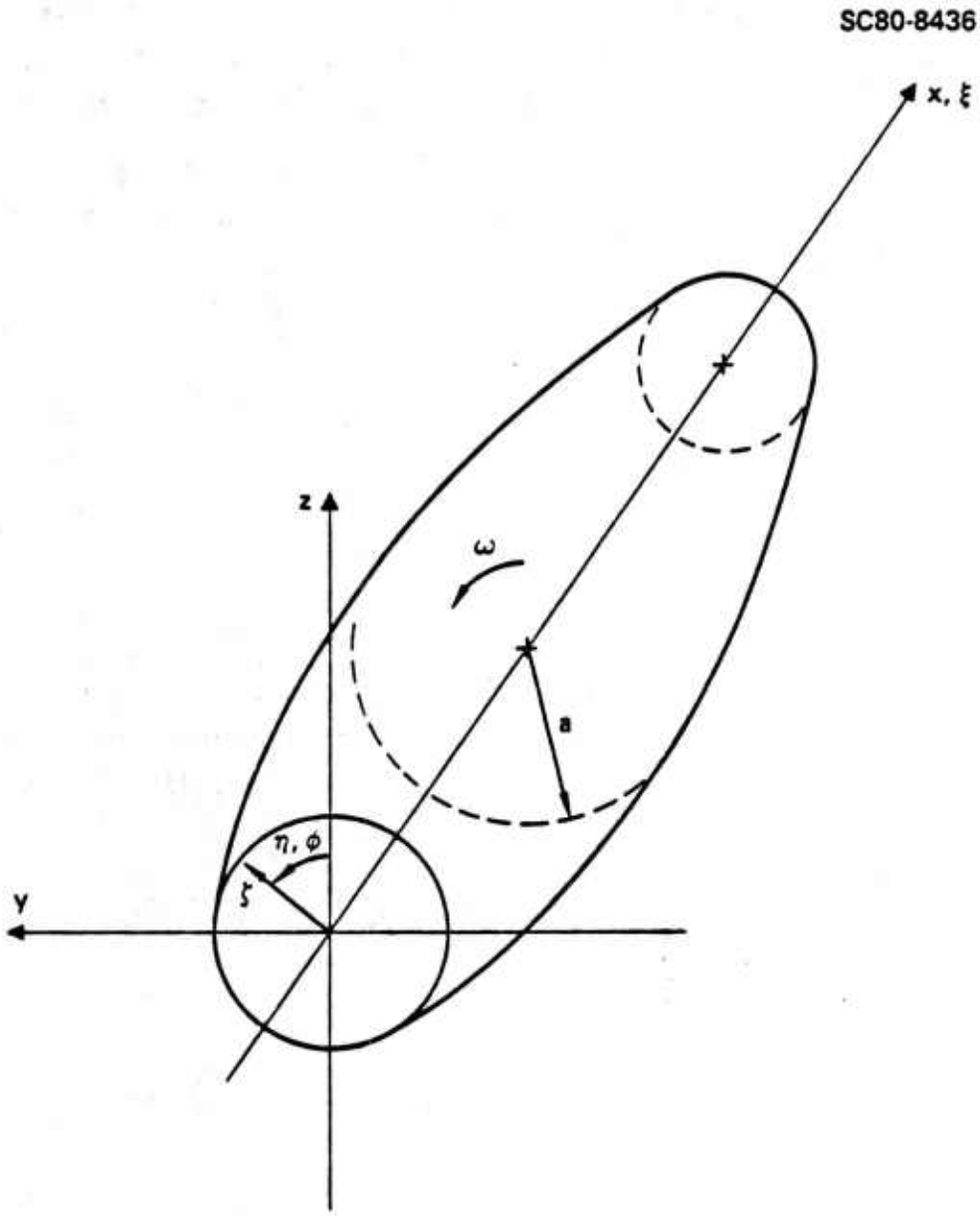

Fig. 1. Sketch of interior flow domain with coordinate definition

and

$$\vec{E}_v = \nu \begin{bmatrix} 0 \\ \xi_x u_\xi + \eta_x u_\eta + \zeta_x u_\zeta \\ \xi_x v_\xi + \eta_x v_\eta + \zeta_x v_\zeta \\ \xi_x w_\xi + \eta_x w_\eta + \zeta_x w_\zeta \end{bmatrix},$$

$$\vec{F}_v = \nu \begin{bmatrix} 0 \\ \eta_y u_\eta + \zeta_y u_\zeta \\ \eta_y v_\eta + \zeta_y v_\zeta \\ \eta_y w_\eta + \zeta_y w_\zeta \end{bmatrix}, \quad \vec{G}_v = \nu \begin{bmatrix} 0 \\ \eta_z u_\eta + \zeta_z u_\zeta \\ \eta_z v_\eta + \zeta_z v_\zeta \\ \eta_z w_\eta + \zeta_z w_\zeta \end{bmatrix} \tag{5}$$

Throughout the above equations, ξ_y and ξ_z were assumed to be zero, while the remaining metrics are given by

$$(\xi_x/J) = 1/(x_\xi J), \quad (\eta_x/J) = z_\xi y_\zeta - y_\xi z_\zeta, \quad (\zeta_x/J) = y_\xi z_\eta - z_\xi y_\eta$$

$$(\eta_y/J) = x_\xi z_\zeta \quad , \quad (\zeta_y/J) = \quad - x_\xi z_\eta$$

$$(\eta_z/J) = \quad - x_\xi y_\zeta, \quad (\zeta_z/J) = x_\xi y_\eta$$

$$\begin{aligned} (\xi_t/J) &= - \ (\xi_x/J)x_\tau \\ (\eta_t/J) &= -(\ (\eta_x/J)x_\tau + (\eta_y/J)y_\tau + (\eta_z/J)z_\tau \ ) \\ (\zeta_t/J) &= -(\ (\zeta_x/J)x_\tau + (\zeta_y/J)y_\tau + (\zeta_z/J)z_\tau \ ) \end{aligned} \tag{6}$$

$$(\ 1/J) = x_\xi(y_\eta z_\zeta - y_\zeta z_\eta)$$

The governing equations are kept in a more manageable form if contravariant velocities are introduced (shown here in the non-scaled form)

$$\begin{aligned} U &= \xi_t + \xi_x u \\ V &= \eta_t + \eta_x u + \eta_y v + \eta_z w \\ W &= \zeta_t + \zeta_x u + \zeta_y v + \zeta_z w \end{aligned} \tag{7}$$

Then, the flux functions are simply written as

$$\hat{E} = J^{-1}\begin{bmatrix} \beta U + \xi_t(p-\beta) \\ uU + \xi_x p \\ vU \\ wU \end{bmatrix}, \quad \hat{F} = J^{-1}\begin{bmatrix} \beta V + \eta_t(p-\beta) \\ uV + \eta_x p \\ vV + \eta_y p \\ wV + \eta_z p \end{bmatrix}, \quad \hat{G} = J^{-1}\begin{bmatrix} \beta W + \zeta_t(p-\beta) \\ uW + \zeta_x p \\ vW + \zeta_y p \\ wW + \zeta_z p \end{bmatrix} \tag{8}$$

Note that even though U, V, and W are introduced, the dependent variables remain p, u, v, w - i.e., the inertial or cartesian velocity components are retained.

The viscous terms have the form

$$\begin{aligned} \hat{E}_v &= (\nu/J)(\nabla\xi\cdot\nabla\xi\ \underline{\underline{I}}_m\ \partial_\xi\vec{D} + \nabla\xi\cdot\nabla\eta\ \underline{\underline{I}}_m\ \partial_\eta\vec{D} + \nabla\xi\cdot\nabla\zeta\ \underline{\underline{I}}_m\ \partial_\zeta\vec{D}) \\ \hat{F}_v &= (\nu/J)(\nabla\eta\cdot\nabla\xi\ \underline{\underline{I}}_m\ \partial_\xi\vec{D} + \nabla\eta\cdot\nabla\eta\ \underline{\underline{I}}_m\ \partial_\eta\vec{D} + \nabla\eta\cdot\nabla\zeta\ \underline{\underline{I}}_m\ \partial_\zeta\vec{D}) \\ \hat{G}_v &= (\nu/J)(\nabla\zeta\cdot\nabla\xi\ \underline{\underline{I}}_m\ \partial_\xi\vec{D} + \nabla\zeta\cdot\nabla\eta\ \underline{\underline{I}}_m\ \partial_\eta\vec{D} + \nabla\zeta\cdot\nabla\zeta\ \underline{\underline{I}}_m\ \partial_\zeta\vec{D}) \end{aligned} \tag{9}$$

where the matrix $\underline{I}_m$ is the modified Identity matrix:

$$\underline{I}_m = \begin{bmatrix} 0 & & & \\ & 1 & & \\ & & 1 & \\ & & & \underline{1} \end{bmatrix} \tag{10}$$

and with the use of orthogonal coordinates (when possible) simplify to

$$\begin{aligned} \hat{E}_v &= (\nu/J)\ (\ \xi_x^2 \qquad\qquad\ )\ \underline{I}_m\ \partial_\xi \vec{D} \\ \hat{F}_v &= (\nu/J)\ (\ \eta_x^2 + \eta_y^2 + \eta_z^2\ )\ \underline{I}_m\ \partial_\eta \vec{D} \\ \hat{G}_v &= (\nu/J)\ (\ \zeta_x^2 + \zeta_y^2 + \zeta_z^2\ )\ \underline{I}_m\ \partial_\zeta \vec{D} \end{aligned} \tag{11}$$

In the above, the equations have been cast in nondimensional form with

$$\begin{aligned} &\tilde{u} = u/u_{ref}\ , \quad \tilde{v} = v/u_{ref}\ , \quad \tilde{w} = w/u_{ref} \\ &\tilde{x} = x/x_{ref}\ , \quad \tilde{y} = y/x_{ref}\ , \quad \tilde{z} = z/z_{ref} \\ &\tilde{t} = t\ u_{ref}/x_{ref} \qquad\qquad , \quad \tilde{p} = p/u_{ref}^2 \\ &\tilde{\nu} = Re^{-1} = \nu/(x_{ref}u_{ref}) \quad , \quad \tilde{\beta} = \beta/u_{ref}^2 \end{aligned} \tag{12}$$

with the subscript ref denoting reference quantities and the $\tilde{}$ are deleted in the governing equations for simplicity. For a spinning cylinder, the usual reference quantities are $x_{ref} = a$, the radius of of the cylinder and $u_{ref} = a\omega$ where ω is the rotational speed.

BOUNDARY CONDITIONS

Boundary conditions require that the velocities U, V, W = 0 at the walls (no slip) if the ξ,η,ζ coordinates are rigidly attached to the shell. Thus, along the walls,

$$u = \dot{x} , \quad v = \dot{y} , \quad w = \dot{z} \tag{13}$$

where $\dot{x}$, $\dot{y}$, and $\dot{z}$ are the velocities of a particle attached to the wall. Alternately, spin about the axis can be taken out of the body motion by setting[7]

$$V = \omega/\phi_{\eta} \tag{14}$$

This latter approach has the advantage of removing changes in the velocity solely due to coordinate rotation.

SUBTRACTING OUT AXISYMMETRIC VARIATION

The equations given above are formulated in terms of cartesian components of velocity. Even for completely spun up flow in a shell that is not coning or precessing, the cartesian velocity components possess circumferential gradients as opposed to cylindrical velocity components which only have zero gradients. This implies that, even to compute the axisymmetric flow after spin up, in the present formulation, one has to solve the entire three-dimensional equations in time. Also, even for mildly non-axisymmetric flows, the number of grid points needed to accurately represent the cartesian velocity components in the circumferential direction is excessive compared to the number necessary for cylindrical components of velocity.

There are two ways of alleviating this problem. One approach is to use cylindrical components of velocity as the dependent variables. This

is described in Section 5. The other approach is to use the current cartesian formulation but to subtract out the true axisymmetric variation.

In subtracting the true axisymmetric variation, the governing equations would be rewritten

$$\partial_\tau \hat{D} + \partial_\xi(\hat{E}-\hat{E}_v) + \partial_\eta(\hat{F}-\hat{F}_a - (\hat{F}_v-\hat{F}_{va})) + \partial_\zeta(\hat{G}-\hat{G}_v) = -(\hat{H}_a-\hat{H}_{va}) \tag{15}$$

where

$$\hat{H}_a-\hat{H}_{av} = J^{-1}\phi_\eta \begin{vmatrix} 0 \\ 0 \\ V[R_\xi(U-\xi_t)\cos\phi - R\phi_\eta(V-\eta_t)\sin\phi \\ + R_\zeta(W-\zeta_t)\cos\phi] - p\sin\phi/(R\phi_\eta) \\ -V[R_\xi(U-\xi_t)\sin\phi + R\phi_\eta(V-\eta_t)\cos\phi \\ + R_\zeta(W-\zeta_t)\sin\phi] - p\cos\phi/(R\phi_\eta) \end{vmatrix} + \nu J^{-1}R^{-2} \begin{vmatrix} 0 \\ 0 \\ v \\ w \end{vmatrix} \tag{16}$$

In Eqs.(15) and (16), the subscript a is used to denote truly axisymmetric terms. The letter R is used to denote the radius of the point under consideration. The quantity $\partial_\eta \hat{F}_a$ is equal to $\hat{H}_a$. However, the term $\partial_\eta \hat{F}_a$ on the left hand side of the equation will be differenced rather than exactly evaluated and it will cancel out the numerical error of differencing $\partial_\eta \hat{F}$ due to axisymmetric

variation. Non-axisymmetric variation in η is retained in the terms $\partial_\eta \hat{F} - \partial_\eta \hat{F}_a$ while the correct axisymmetric variation is held in $\hat{H}_a$. To use this approach, metrics must be evaluated via the procedure explained in Ref. 7 (Eq. 7). Note that the viscous terms also contribute to the true axisymmetric variation.

Once either of these approaches are incorporated, it becomes an easy matter to build a two-dimensional option into the computer code by bypassing the η or azimuthal inversions. This option becomes even easier to achieve because the present computer code comprises a single index array structure. The two-dimensional program would allow the calculation of high Reynolds number axisymmetric spin up to proceed until the three-dimensional perturbations of the body motion need to be introduced. It can also be used as an economic code for optimizing numerical dissipation, grid stretching and the use of variable step sizes. The axisymmetric code will also be used to compute solutions to compare with other known solutions such as those presented by Kitchens[3].

4. NUMERICAL METHOD FOR CARTESIAN VARIABLE FORMULATION

The numerical method described below is presented in detail in Ref. 5. The approximate factorization difference equations in delta form (or increment form) are given below assuming orthogonal coordinates in order to simplify writing the viscous terms.

$$
\begin{aligned}
&[\underline{I} + hJ^{n+1}(\delta_\xi \underline{\hat{A}}^n - \overline{\delta}_\xi \gamma_1 \underline{I}_m \overline{\delta}_\xi) + \varepsilon_i \nabla_\xi \Delta_\xi \,] \\
&\cdot[\underline{I} + hJ^{n+1}(\delta_\eta \underline{\hat{B}}^n - \overline{\delta}_\eta \gamma_2 \underline{I}_m \overline{\delta}_\eta) + \varepsilon_i \nabla_\eta \Delta_\eta \,] \\
&\cdot[\underline{I} + hJ^{n+1}(\delta_\zeta \underline{\hat{C}}^n - \overline{\delta}_\zeta \gamma_3 \underline{I}_m \overline{\delta}_\zeta) + \varepsilon_i \nabla_\zeta \Delta_\zeta \,](\vec{D}^{n+1} - \vec{D}^n) \\
&= (\underline{I} - \underline{I}_m)(p^* - p^n) \\
&- (1 - J^{n+1}/J^n)\vec{D}^n \\
&- \Delta\tau J^{n+1}(\delta_\xi \hat{E}^n + \delta_\eta \hat{F}^n + \delta_\zeta \hat{G}^n - \overline{\delta}_\xi \gamma_1 \underline{I}_m \overline{\delta}_\xi \vec{D}^n - \overline{\delta}_\eta \gamma_2 \underline{I}_m \overline{\delta}_\eta \vec{D}^n - \overline{\delta}_\zeta \gamma_3 \underline{I}_m \overline{\delta}_\zeta \vec{D}^n) \\
&- \varepsilon_e[(\nabla_\xi \Delta_\xi)^2 + (\nabla_\eta \Delta_\eta)^2 + (\nabla_\zeta \Delta_\zeta)^2 \,] \vec{D}^n
\end{aligned}
\tag{17}
$$

where

$$\gamma_1 = (\nu/J)\xi_x^2$$

$$\gamma_2 = (\xi_x^2 + \xi_y^2 + \xi_z^2)(\nu/J)$$

$$\gamma_3 = (\eta_x^2 + \eta_y^2 + \eta_z^2)(\nu/J)$$

ε_e and ε_i are $O(\Delta\tau)$

$h = \Delta\tau$ for Euler time differencing

$h = \Delta\tau/2$ for trapezoidal time differencing

$$\nabla_\xi \vec{D} \equiv \vec{D}_j - \vec{D}_{j-1} \quad , \quad \Delta_\eta \vec{D} \equiv \vec{D}_{k+1} - \vec{D}_k \quad ,$$

$$\delta_\zeta \vec{D} \equiv (\vec{D}_{\ell+1} - \vec{D}_{\ell-1})/(2\Delta\zeta) \ ,$$

$$\overline{\delta}_\eta \alpha \overline{\delta}_\eta \vec{D} \equiv \{(\alpha_{k+1}+\alpha_k)(\vec{D}_{k+1}-\vec{D}_k) - (\alpha_k+\alpha_{k-1})(\vec{D}_k-\vec{D}_{k-1})\}/\{2(\Delta\eta)^2\} \ , \text{ etc.}$$

and , etc. have similar definitions save for which is fourth order accurate, i.e.,

$$\delta_\eta \vec{D} \equiv (\vec{D}_{k+2} - 4\vec{D}_{k+1} + 6\vec{D}_k - 4\vec{D}_{k-1} + \vec{D}_{k-2})/(12\Delta\eta)$$

In the above equation, all of the metrics are kept at time level $n+\frac{1}{2}$ for the case of coordinates moving with time. The metrics are centrally differenced with those in the azimuthal direction being fourth order accurate and the others being second order accurate. Also in the above equation describing the implicit approximate factorization procedure, the equations have been locally linearized in time and the Jacobian matrices for the inviscid terms are obtained from

$$\underline{\hat{A}}, \underline{\hat{B}}, \underline{\hat{C}} = \begin{bmatrix} L_0 & L_1 & L_2 & L_3 \\ L_1 & Q+L_1u & L_2u & L_3u \\ L_2 & L_1v & Q+L_2v & L_3v \\ L_3 & L_1w & L_2w & Q+L_3w \end{bmatrix} \tag{18}$$

where $Q = L_0 + L_1u + L_2v + L_3w$

and $L_0 = \xi_t$, $L_1 = \xi_x$, $L_2 = \xi_y$, $L_3 = \xi_z$ to obtain Matrix $\underline{\hat{A}}$, etc.

Equivalent matrices for the viscous terms may be derived easily but are avoided by using orthogonal coordinates when possible. The terms multiplied by the coefficients ϵ_e and ϵ_i are the explicitly and implicitly added smoothing terms which help stabilize the calculations.

SATISFYING THE CONTINUITY EQUATION

It can be shown that when $\beta = O(1/(\Delta\tau))$, the equation (1) along with the definitions (2) will satisfy the continuity equation upto first order accuracy. For better satisfaction of the continuity equation, the finite difference equations (14) are solved atleast twice every time step. In the first iteration, p^* is set to be = p^n and β is chosen to be of the order of $1/(\Delta\tau)$. For subsequent iterations, p^* is set to the value of p^{n+1} predicted in the previous iteration and β is set to unity. This strategy serves the double purpose of satisfying the continuity equation better (when $p^* - p^n = p^{n+1} - p^n$, the continuity equation is satisfied exactly) and removing errors due to large values of β contaminating the momentum equations due to approximate factorization. For more details, see Appendix A of Ref. 5.

5. RESULTS FOR AXISYMMETRIC SPIN-UP USING CARTESIAN VARIABLE FORMULATION

Several axisymmetric test cases involving pure spin up from rest were analyzed in order to verify the method described in the previous Sections. Results were compared with solutions obtained using the code developed by Kitchens[3]. These latter solutions were provided by Sedney and Gerber of BRL (private communication). This Section is devoted to a description of the results obtained using the cartesian variable formulation. Results using the cylindrical variable formulation will be presented in the next Section after presenting the governing equations.

GRID CLUSTERING

Near the end and side walls of the cylindrical container, adequate flow field resolution is especially important to accurately account for the predominantly viscous effects in the boundary layers. To achieve this resolution, the same formulae used by Kitchens[3] to cluster more grid points near the end walls and side wall were employed. For example, in the radial direction, the radial position of a grid point corresponding to a uniformly spaced coordinate ζ was defined by

$$r = b \frac{\{(b+1)/(b-1)\}^{\zeta} - 1}{\{(b+1)/(b-1)\}^{\zeta} + 1} \qquad (19)$$

(the parameter b is the control to achieve desired clustering)

where ζ and r range from zero to one. The axial direction was similarly treated.

EVOLUTION OF SPIN-UP FLOW

Results are now presented to illustrate the evolution of the flow field in a cylindrical spinning cavity spun up impulsively from rest. The first case considered was a cylinder of aspect ratio unity (aspect ratio is the ration of cylinder half height to its radius) with a fluid of Reynolds number 10,000 based on the cylinder radius and rotational speed (Reynolds number = $\omega a^2/\nu$; see Eq. (12) for notation). The finite difference grid employed for this case is shown in Figure 2 for half the cylinder (31 x 31 points). In this and the following figures, the axis labelled R denotes the radial coordinate and the axis labelled Z corresponds to the axial coordinate (contrary to the convention used in Fig. 1).

The in-plane (radial and axial) velocity field is plotted in Fig. 3a from the solution after 125 steps at a non-dimensional time step of 0.25 (non-dimensional time $\tau = 31.25$). The maximum in-plane velocity component was ~ 0.15 and a length segment of 0.075 units was chosen to represent this magnitude of velocity. All velocity vectors were scaled with respect to this value. Arrows were drawn centered at each grid point with their length representing the magnitude of the velocity there and the orientation depicting direction of velocity. While there is very little action in most of the cylinder, the fluid particles close to the end walls (axial ends) are clearly seen to be accelerated outward. Two close ups of the same plot focusing on one corner are shown in Figs. 3b and 3c for better clarity. The same length scales are used in all velocity vector plots (a magnitude of 0.15 is scaled to a length of 0.075) for this case to enable easy, quantitative visualization of the flow processes. Figures 3d-3h show the decay in the magnitude of the in-plane velocity field as the fluid spins up and approaches the steady state of solid body rotation.

It is also interesting to trace the evolution of the azimuthal

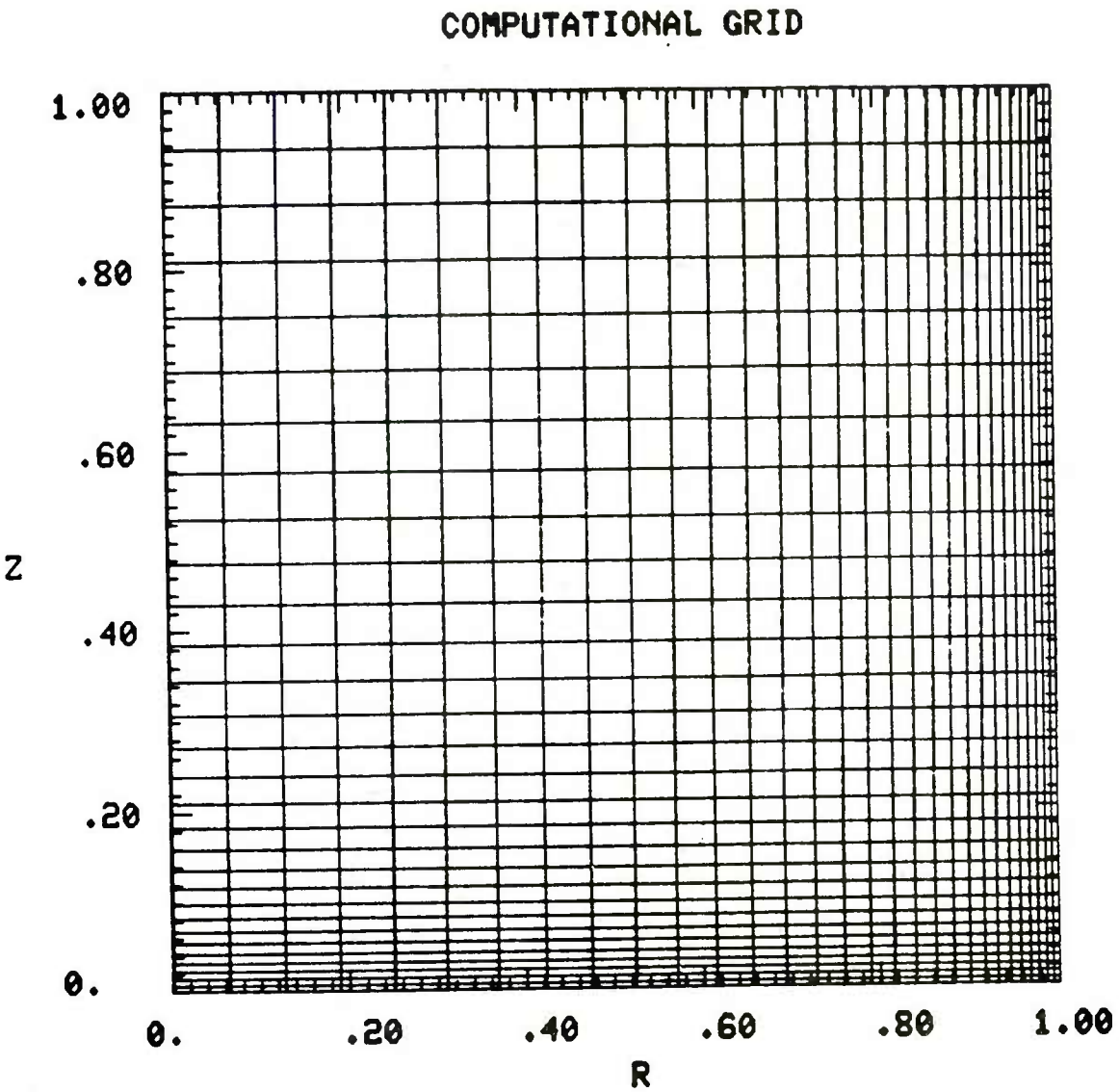

Fig. 2. Computational Grid for Reynolds number of 10,000.

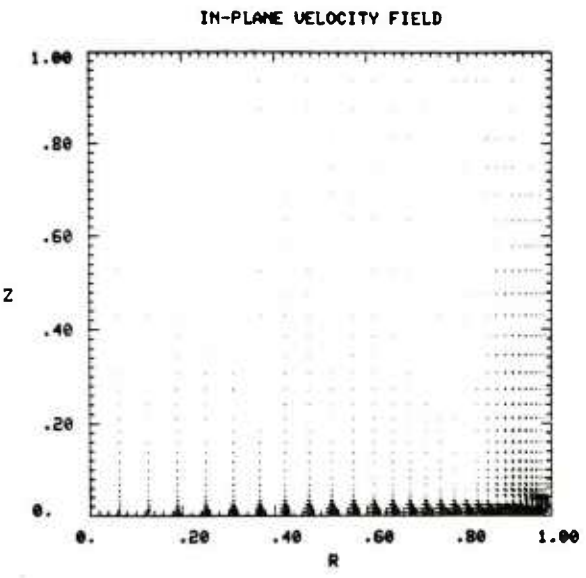

Fig. 3a. Time = 31.25

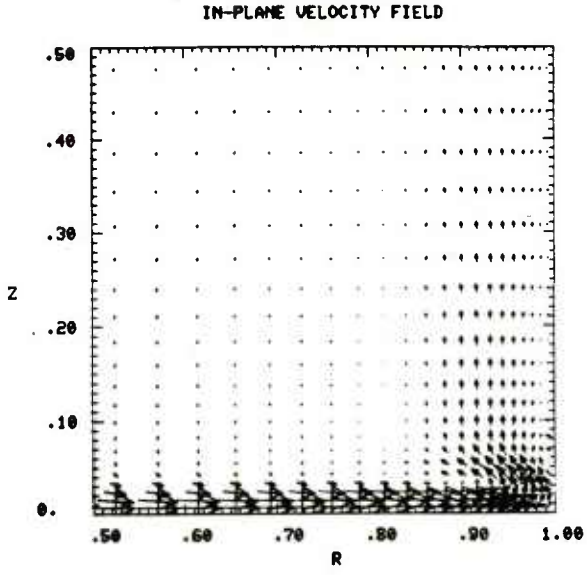

Fig. 3b. Close up of Fig. 3a

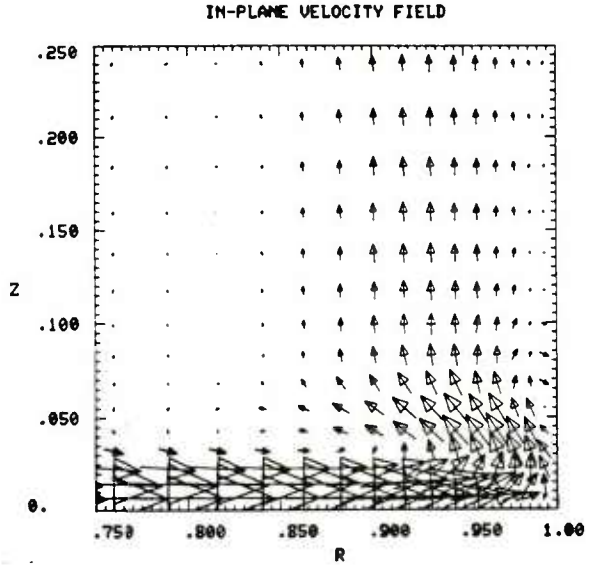

Fig. 3c. Close up of Fig. 3b

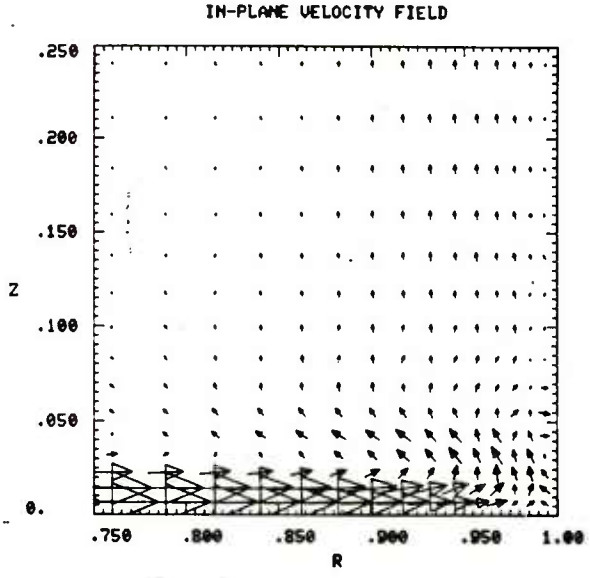

Fig. 3d. Time = 62.5

Fig. 3. In-plane velocity field
Reynolds Number = 10,000. (page 1 of 2)

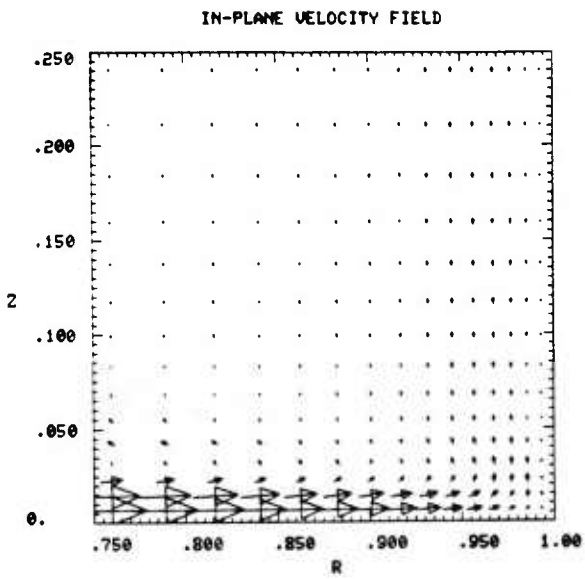

Fig. 3e. Time = 93.75

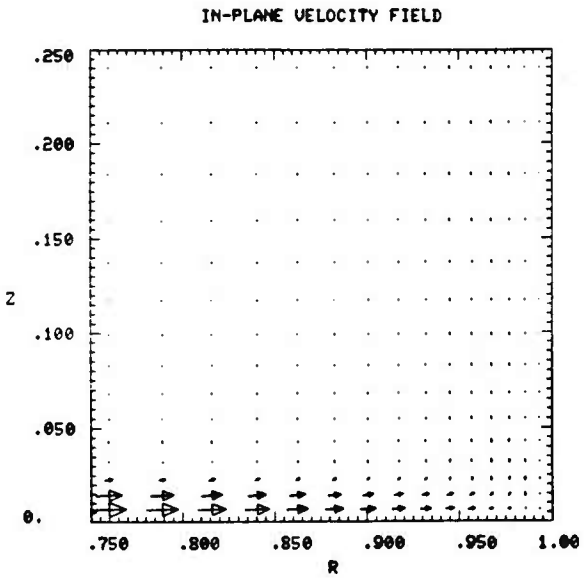

Fig. 3f. Time = 156.25

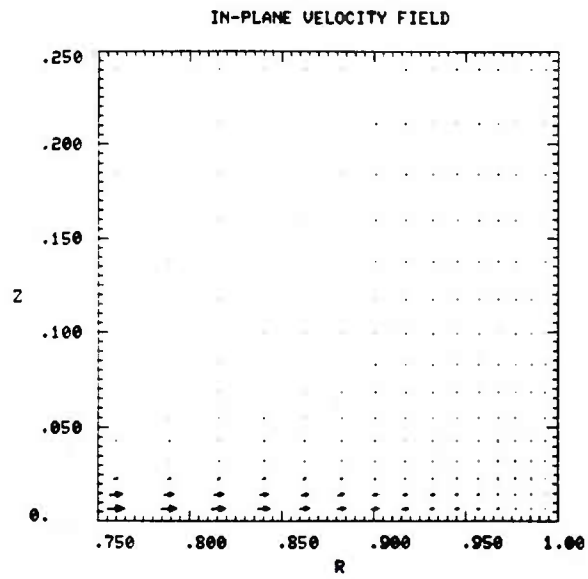

Fig. 3g. Time = 218.75

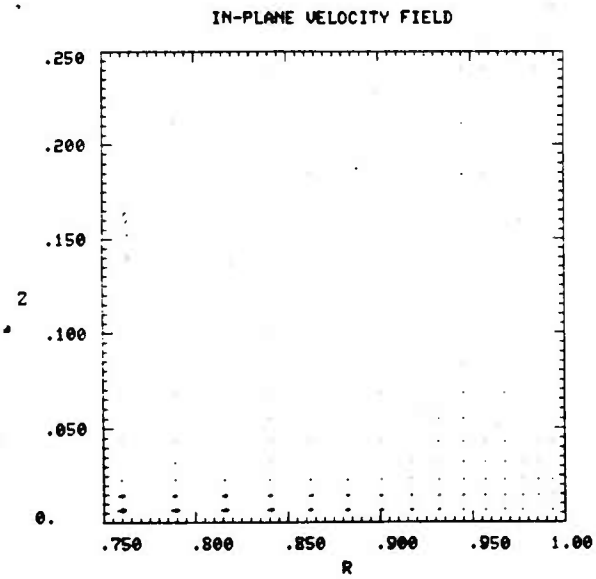

Fig. 3h. Time = 281.25

Fig. 3. (concluded)

velocity distribution. The sequence of Figs. 4a - 4f follow the progression of this velocity component as the flow field develops towards solid body rotation. The minimum contour level shown is 0.05 and the maximum value is 1.0 with increments between levels of 0.05.

A stream-function was defined by

$$\begin{aligned} \partial(\psi)/\partial(\text{radial coordinate}) &= (\text{axial velocity}) \\ \partial(\psi)/\partial(\text{axial coordinate}) &= -(\text{radial velocity}) \end{aligned} \tag{20}$$

and thus

$$\nabla^2\psi = \text{vorticity} \tag{21}$$

Streamline plots were drawn at a sequence of time steps and are displayed in Figs. 5a - 5c. Tangents drawn to these contours must be parallel to the in-plane velocity at that point and it is interesting to observe the vortex core move from the corner between end and side walls radially inward as the flow-field develops.

Similar sets of plots are shown in Figures 6 - 9 for a Reynolds number of 1,000. Figure 6 displays the computational grid of points (31 x 31). A less fine clustering of points is evident compared to the grid for Reynolds number 10,000. The development of the in-plane velocity field and the azimuthal velocity contours are portrayed in Figs. 7a - 7c and Figs. 8a - 8b respectively after 250 and 500 steps at a step size of 0.25. Streamlines are drawn after 250 steps in Fig. 9. This lower Reynolds number case is almost fully spun-up to the solid body state of rotation after only 500 steps. This is in contrast to the first case which converges much more slowly to the asymptotic steady state.

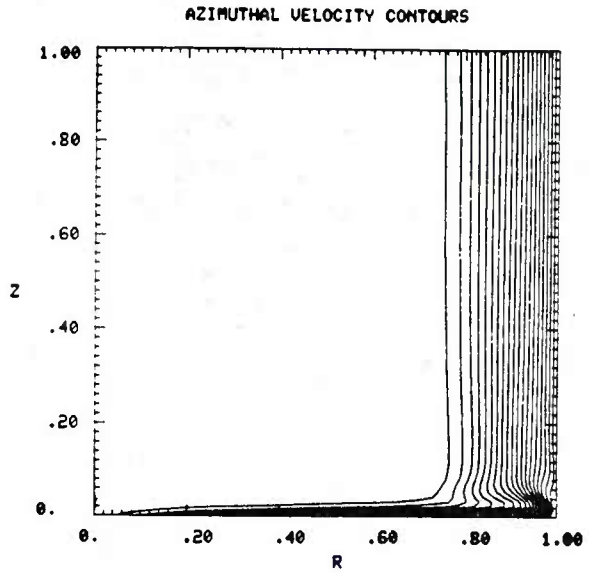

Fig. 4a. Time = 31.25

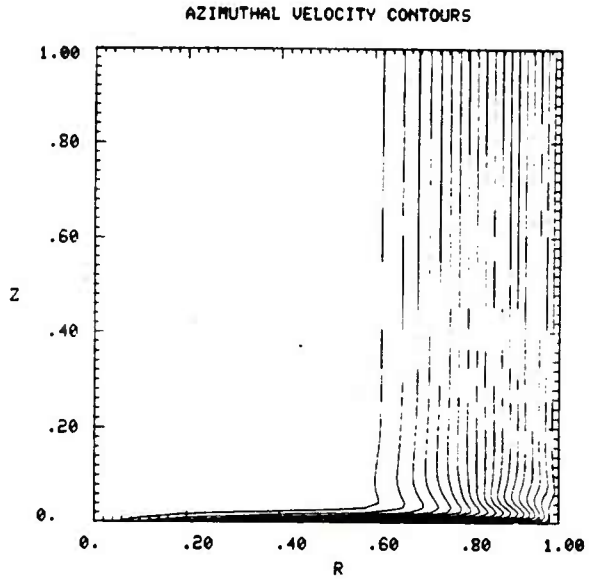

Fig. 4b. Time = 62.5

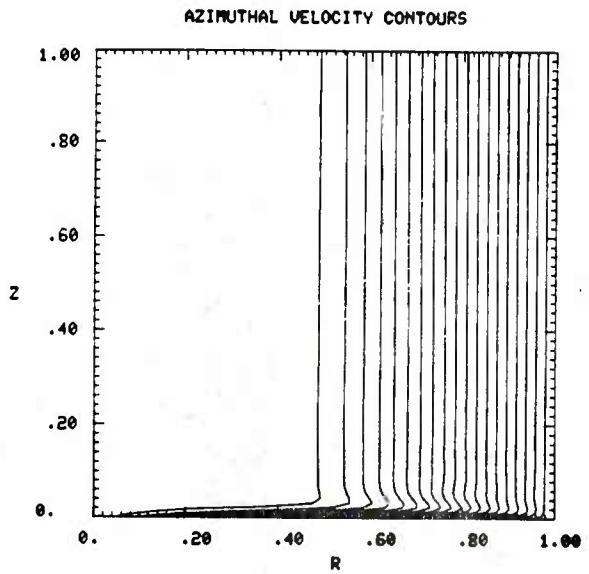

Fig. 4c. Time = 93.75

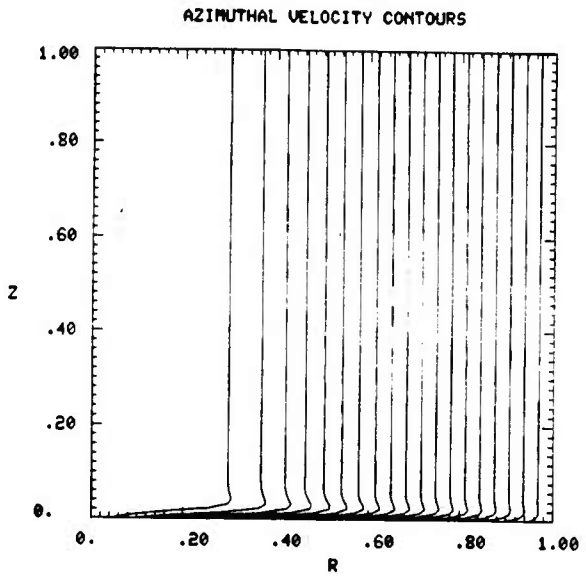

Fig. 4d. Time = 156.25

Fig. 4. Azimuthal velocity plots for Reynolds number 10,000

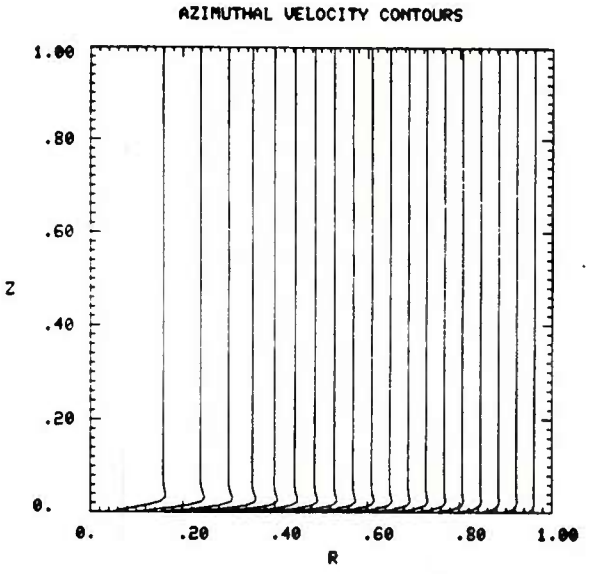

Fig. 4e. Time = 218.75

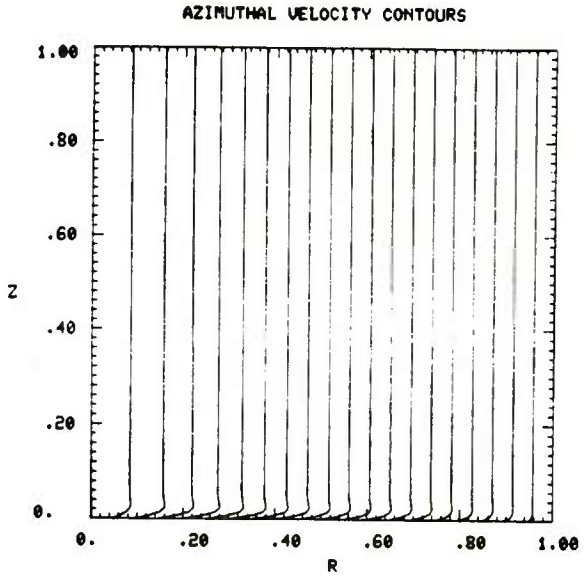

Fig. 4f. Time = 281.25

Fig. 4. (concluded)

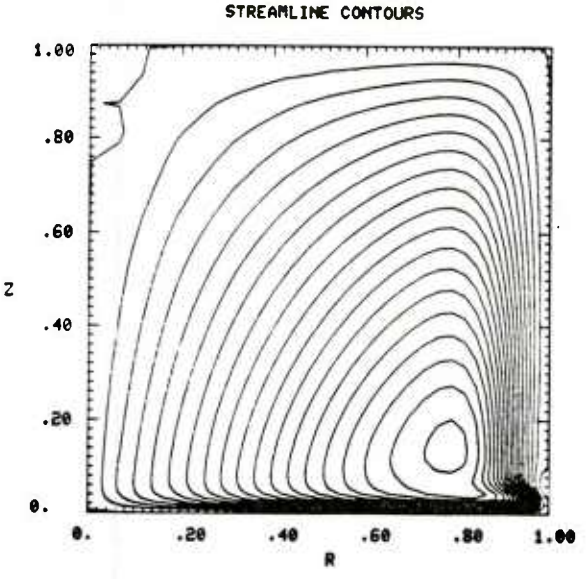

Fig. 5a. Time = 31.25

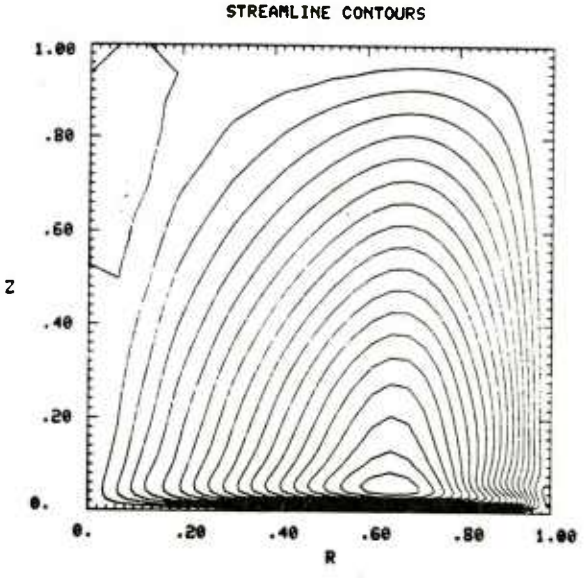

Fig. 5b. Time = 62.5

Fig. 5. Streamline contour plots for Reynolds number 10,000 (page 1 of 2)

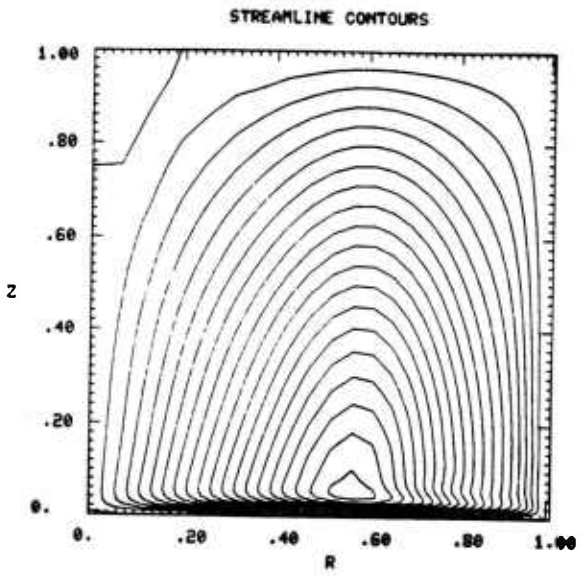

Fig. 5c. Time = 93.75

Fig. 5. (concluded)

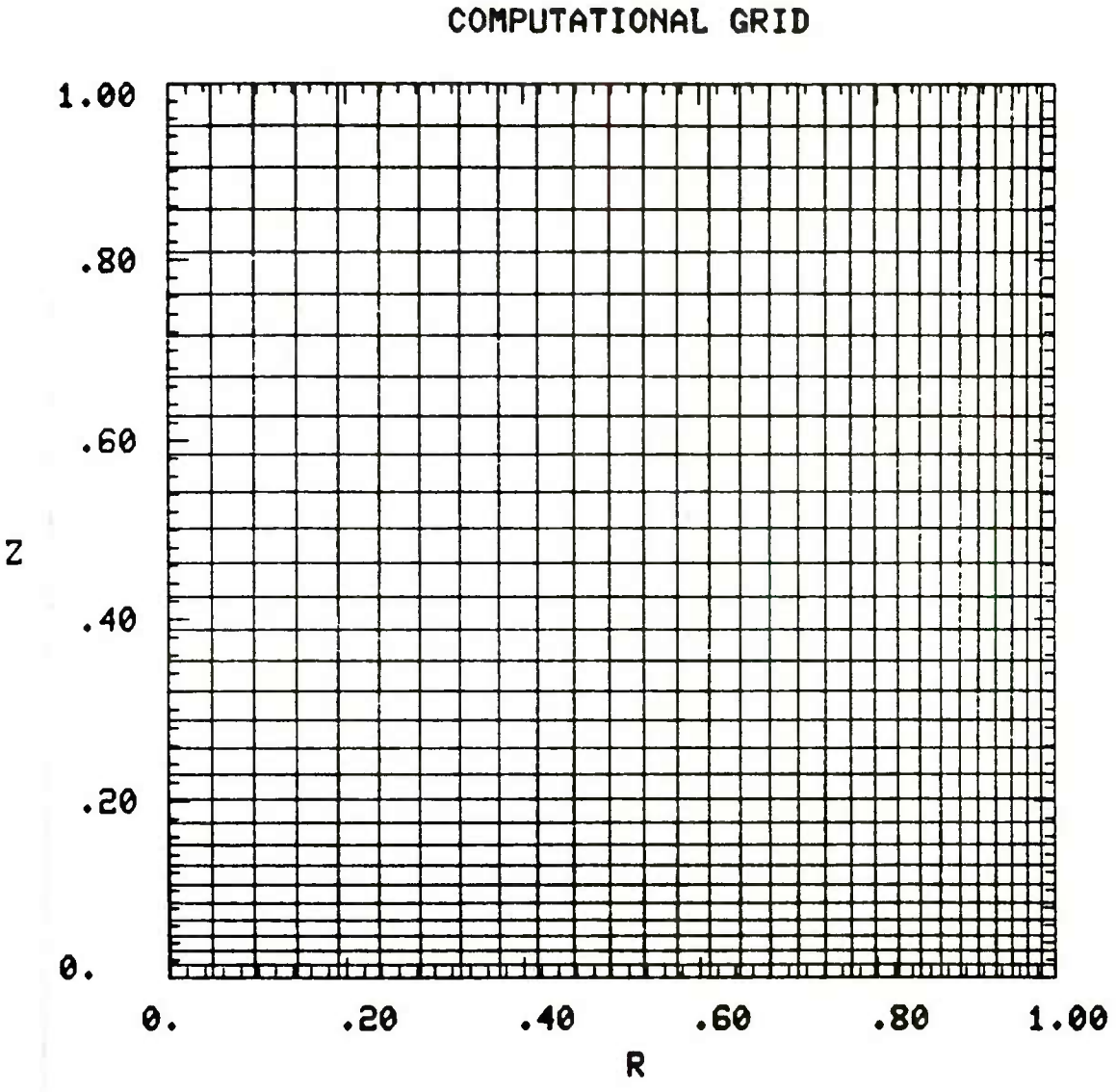

Fig. 6. Computational grid for Reynolds number 1,000

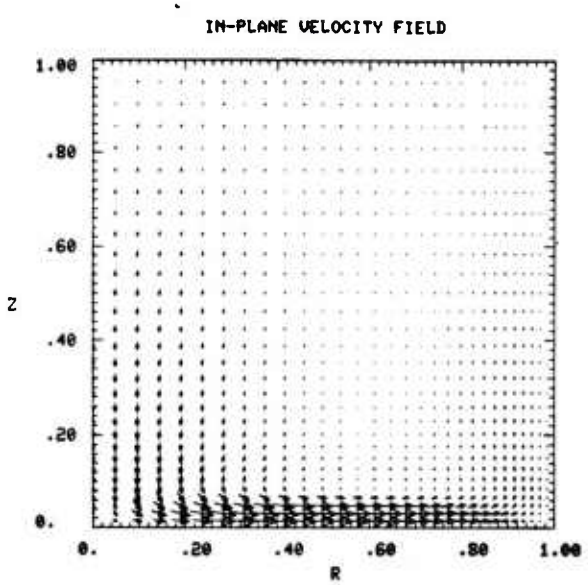

Fig. 7a. Time = 62.5

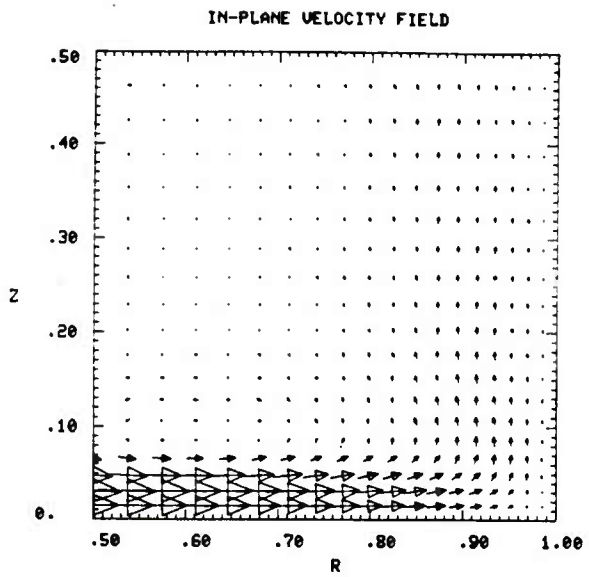

Fig. 7b. Close up of Fig. 7a

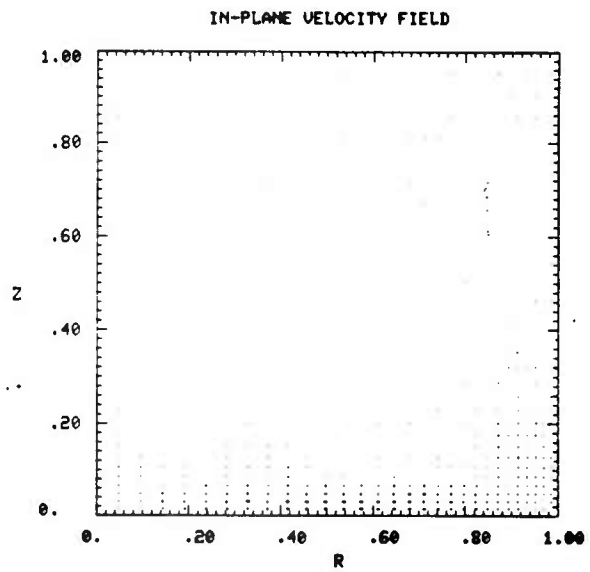

Fig. 7c. Time = 125

Fig. 7. In-plane velocity field for Reynolds number 1,000.

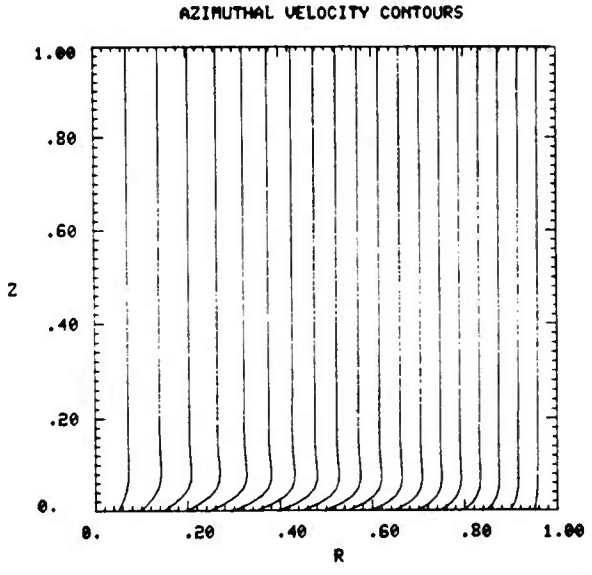

Fig. 8a. Time = 62.5

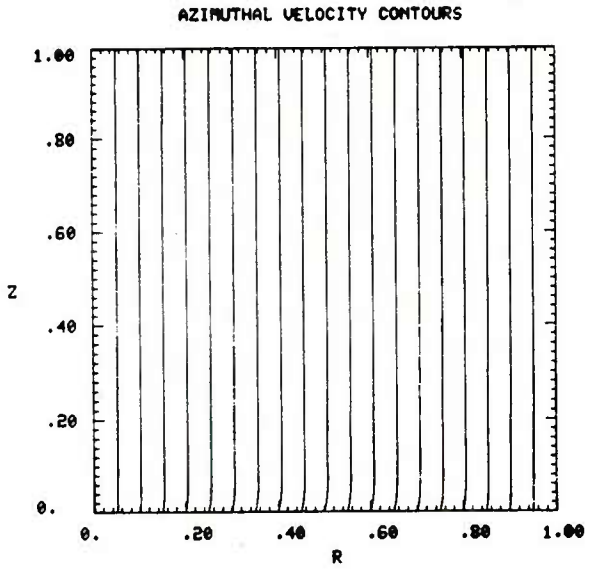

Fig. 8b. Time = 125.0

Fig. 8. Azimuthal velocity plots for Reynolds number 1,000

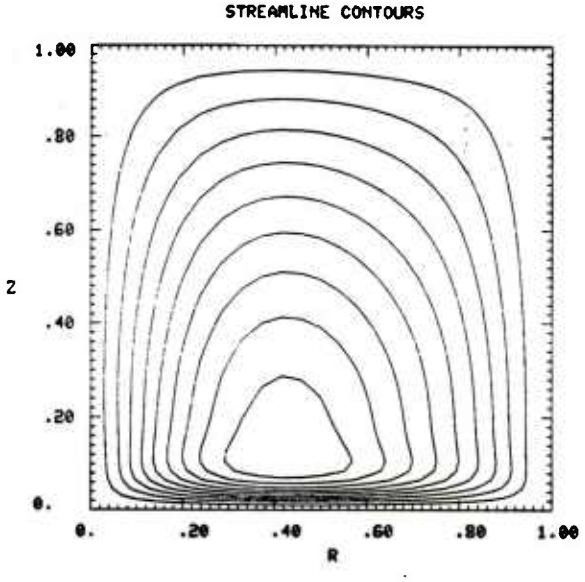

Fig. 9. Streamline contours at Time = 62.5 for Reynolds number 1,000.

COMPARISON WITH RESULTS FROM KITCHENS' CODE

A series of comparisons are now made between the results from the method under evaluation and the code developed by Kitchens[3]. For Reynolds number 10,000 Figs. 10a - 10d compare the two solutions at various axial locations by plotting the radial variation of azimuthal velocity. For these plots, $\tau = 62.5$ with $\Delta\tau = 0.10$. The aspect ratio of the cylinder was unity. First order time accuracy was used along with two iterations every time step to correct the error in satisfying the continuity equation. The two solutions match well, even if not exactly.

A time history of the azimuthal velocity at one point (radial location = 0.9, axial location = 1.0) is shown in Fig. 11. At time $\tau = 62.5$, points from this figure correspond to points from Fig. 10d. Looking at Fig. 11, independently of Figs. 10, it appears like the present solution is lagging behind Kitchens' solution. But , comparing Figs. 10 and 11, it is seen that the time history trends match well if not superbly.

Similar comparisons are made for Reynolds number 1,000 in Figs. 12 and 13 at two non-dimensional times of 62.5 and 125 with a non-dimensional time step of 0.25. Greater smoothing was required for this larger time step and compromised the solution accuracy at $\tau = 62.5$. At the later time of 125.0, the fluid has almost fully spun up and the discrepancy between the two solutions is very minor.

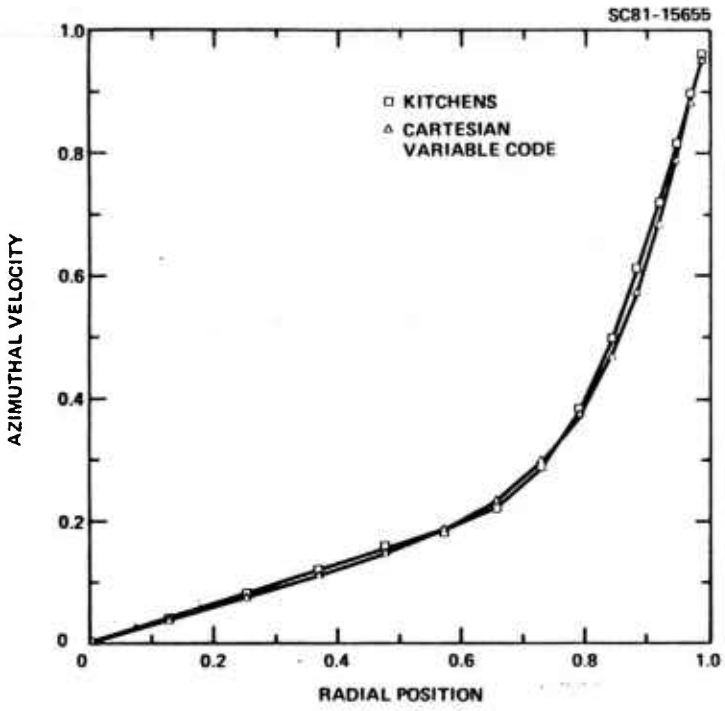

Fig. 10a. Axial location = 0.0145

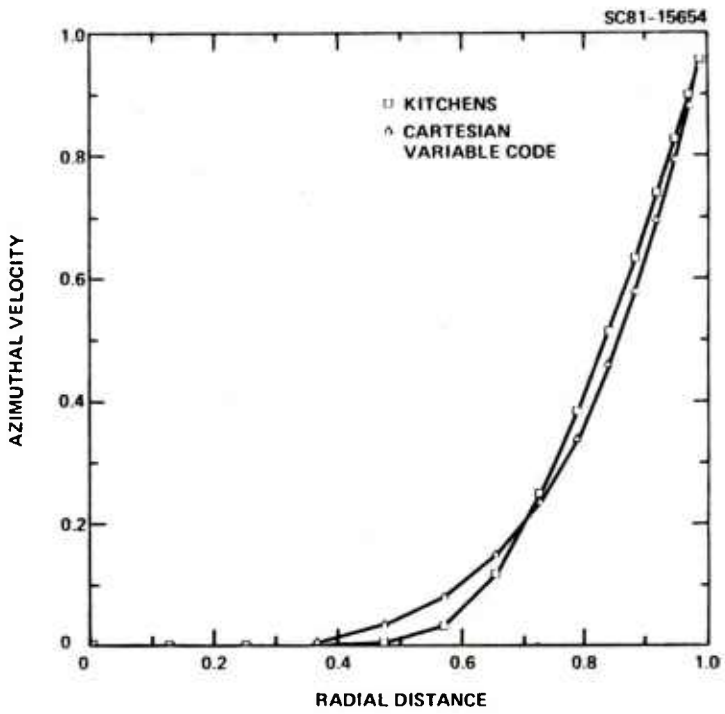

Fig. 10b. Axial location = 0.211

Fig. 10. Comparison of azimuthal velocity profiles for Reynolds number 10,000 and Time = 62.5 (page 1 of 2)

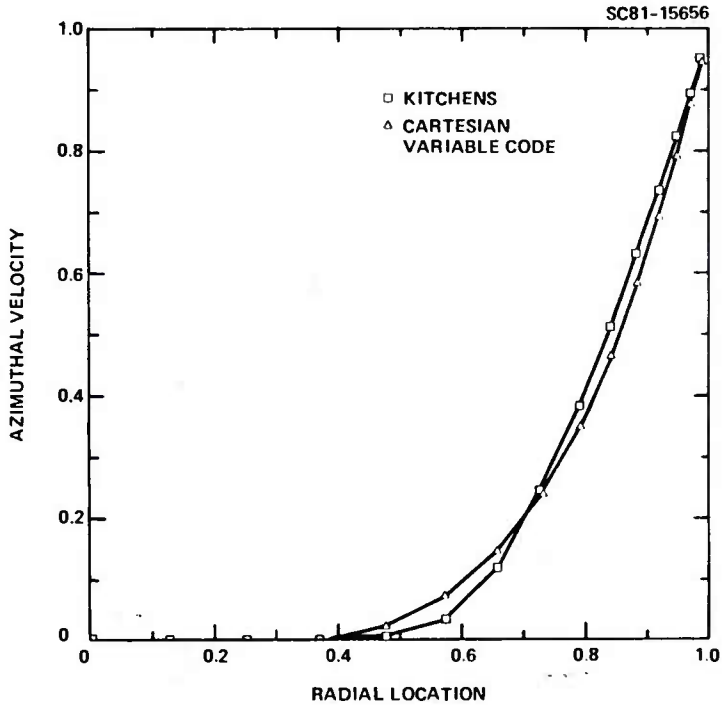

Fig. 10c. Axial location = 0.5255

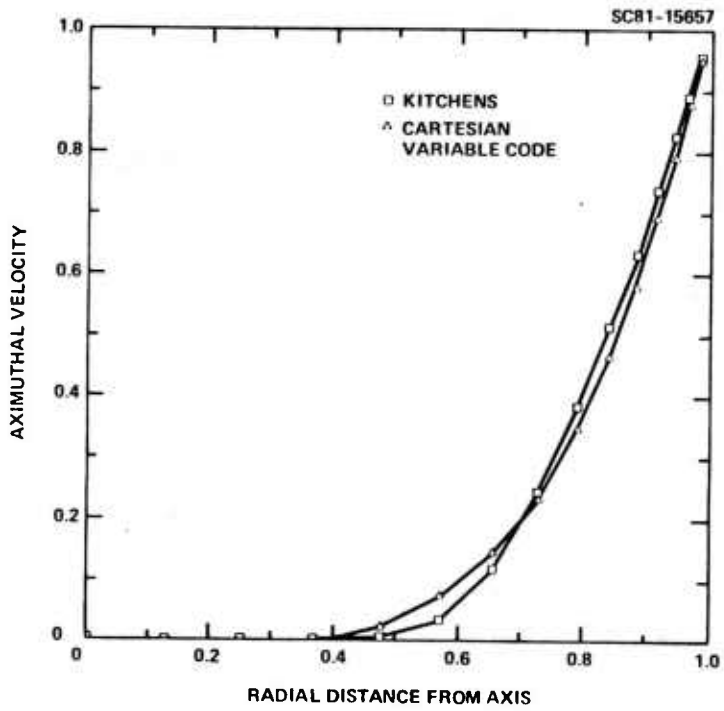

Fig. 10d. Axial location = 1.0

Fig. 10. (concluded)

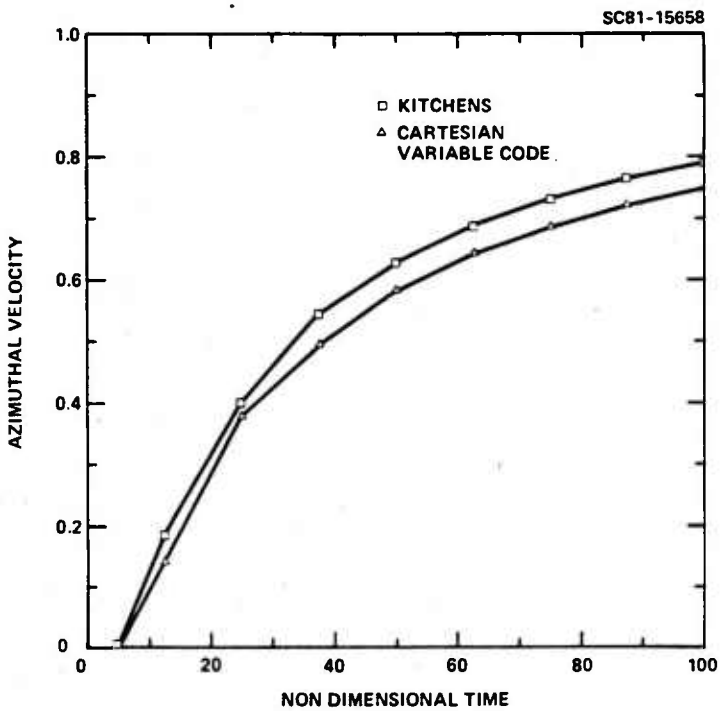

Fig. 11. Time history of azimuthal velocity at axial location of 1.0 and radial location of 0.9.

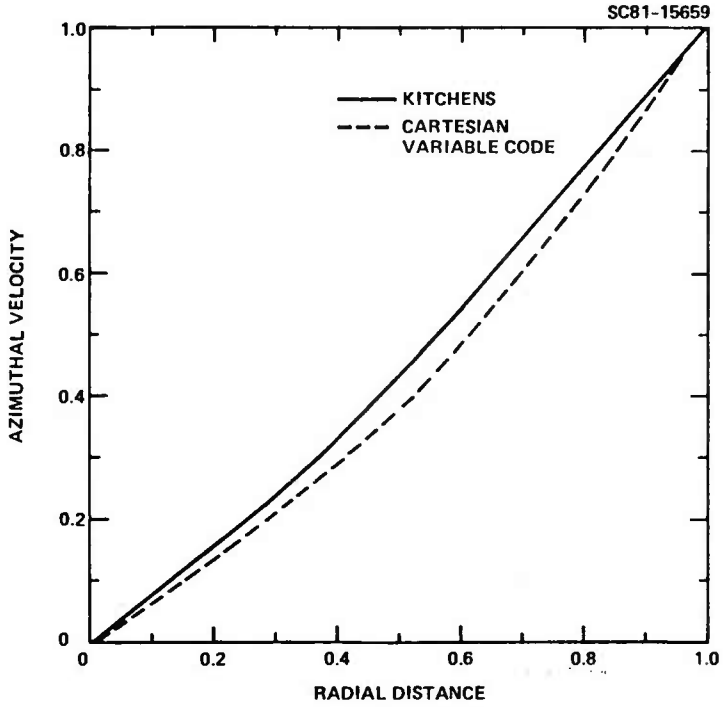

Fig. 12a. Axial location = 0.06621

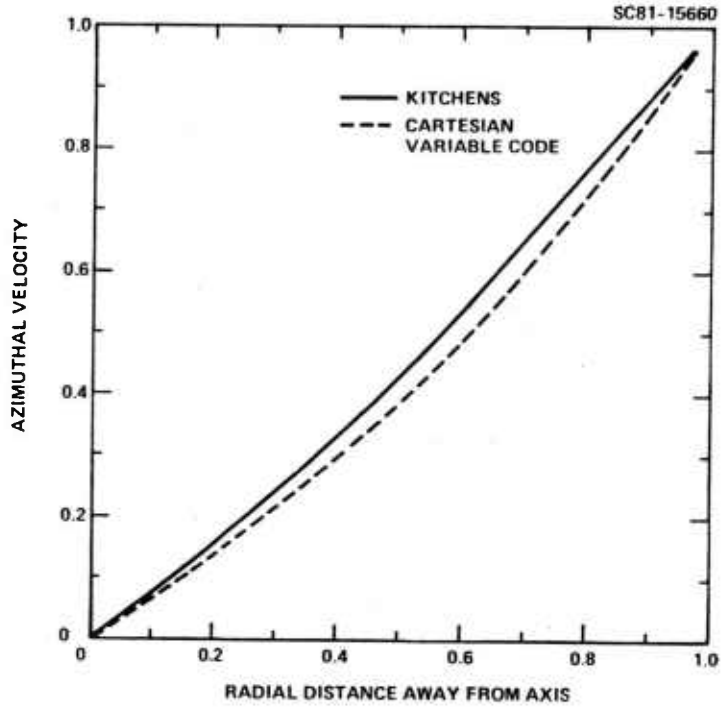

Fig. 12b. Axial location = 1.0

Fig. 12. Comparison of azimuthal velocity profiles for Reynolds number 1,000 at Time = 62.5

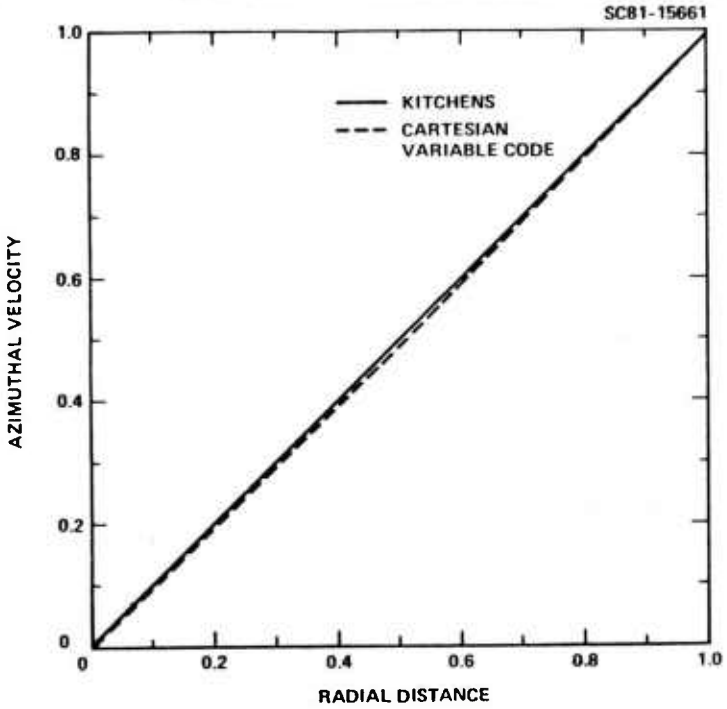

Fig. 13a. Axial location = 0.06621

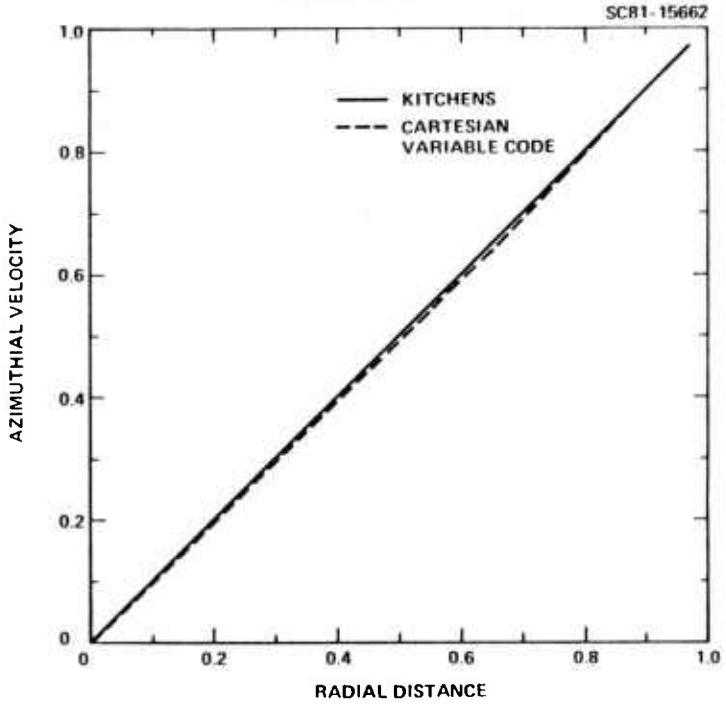

Fig. 13b. Axial location = 1.0

Fig. 13. Comparison of azimuthal velocity profiles for Reynolds number 1,000 at Time = 125.0

6. CYLINDRICAL VARIABLE FORMULATION

The governing Navier-Stokes momentum and continuity equations may be written in non-divergence form in cylindrical variables as

Continuity equation

$$\partial_r u + (1/r)\partial_\theta v + \partial_z w + u/r = 0 \qquad (22a)$$

Momentum equations

$$\partial_t u+u\partial_r u+(v/r)\partial_\theta u+w\partial_z u-v^2/r+ \quad \partial_r p = \nu(\nabla^2 u-(2/r^2)\partial_\theta v-u/r^2) \qquad (22b)$$

$$\partial_t v+u\partial_r v+(v/r)\partial_\theta v+w\partial_z v+uv/r+(1/r)\partial_\theta p = \nu(\nabla^2 v+(2/r^2)\partial_\theta u-v/r^2)$$

$$\partial_t w+u\partial_r w+(v/r)\partial_\theta w+w\partial_z w \quad + \quad \partial_z p = \nu(\nabla^2 w \quad)$$

where,

$$\nabla^2 = \partial_r^2 + (1/r)\partial_r + (1/r^2)\partial_\theta^2 + \partial_z^2$$

r	=	radial	u	=	radial velocity
θ	=	azimuthal coordinate ,	v	=	azimuthal velocity
z	=	axial coordinate ,	w	=	axial velocity

Once again, the continuity equation is modified by the addition of transient terms for pressure

$$\partial_t p + \beta(\partial_r u + (1/r)\partial_\theta v + \partial_z w + u/r) = \partial_t p^* \qquad (22c)$$

These equations were coded into an implicit factorization procedure modified from the method presented in Section 4. The non-conservation form allowed easy use of upwind differencing of the convective terms, thus eliminating the need for artificial smoothing of the type used in Section 4 and avoiding dissipation in the continuity equation altogether. The results that will now be presented for axisymmetric spin up show a marked improvement over the results using the cartesian variables. However, it is too soon to identify specific differences between the two methods that cause this improvement.

RESULTS

The parameters of the first case discussed are: Reynolds number = 1,000, aspect ratio = 1.0. Comparisons between solutions from Kitchens' method and the current cylindrical variable formulation are made in Figs. 14 - 15 at two axial locations ($z = 0.0662$, $z = 1.0$) at two time levels (250 steps and 500 steps with step size = 0.25). A good match is observed, better than the agreement for the results using the cartesian variable formulation.

The Reynolds number is 10,000 and the aspect ratio is unity for the next case considered. Results are compared at two axial locations ($z=0.0324$ and 1.0) and three time levels (250, 500, 1000 steps with step size = 0.25) in Figs. 16, 17, and 18. Once again, better agreement between the two solutions is seen compared to the results of the previous section. The improvement is in spite of using a larger time step than used for the cartesian variable formulation.

The effect of different values of the parameter β and the time accuracy are plotted in Figs. 19 and 20. Both β and the time accuracy are seen to have negligible influence on the results.

Finally, as a check to determine any Reynolds number limits (spin rate limits are related to Reynolds number limits) on the

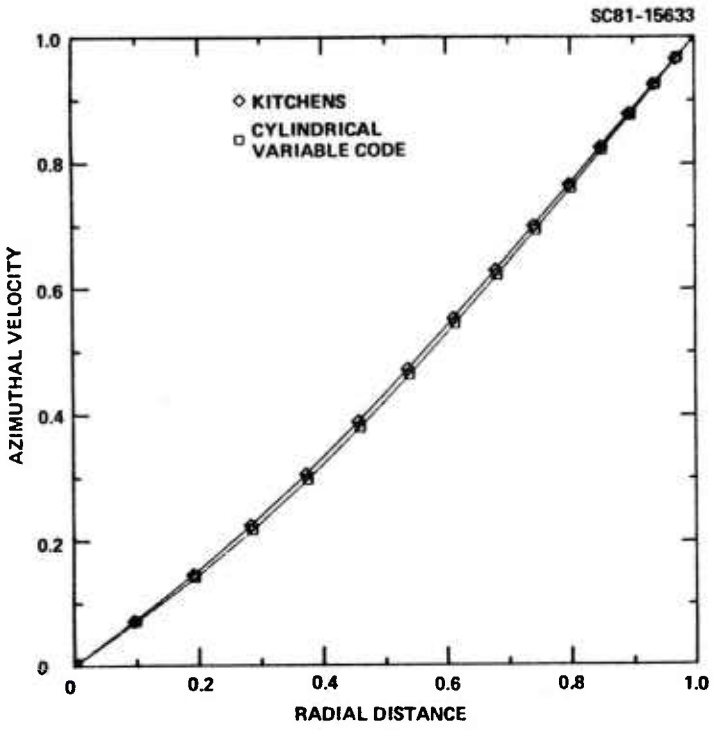

Fig. 14a. Axial location = 0.0662

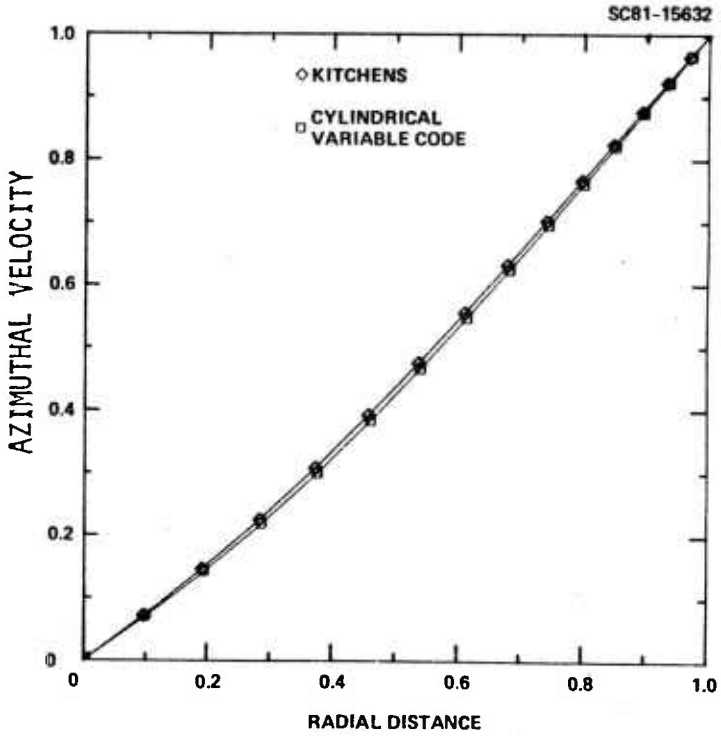

Fig. 14b. Axial location = 1.0

Fig. 14. Comparison of azimuthal velocity profiles for Reynolds number 1,000 at Time = 62.5

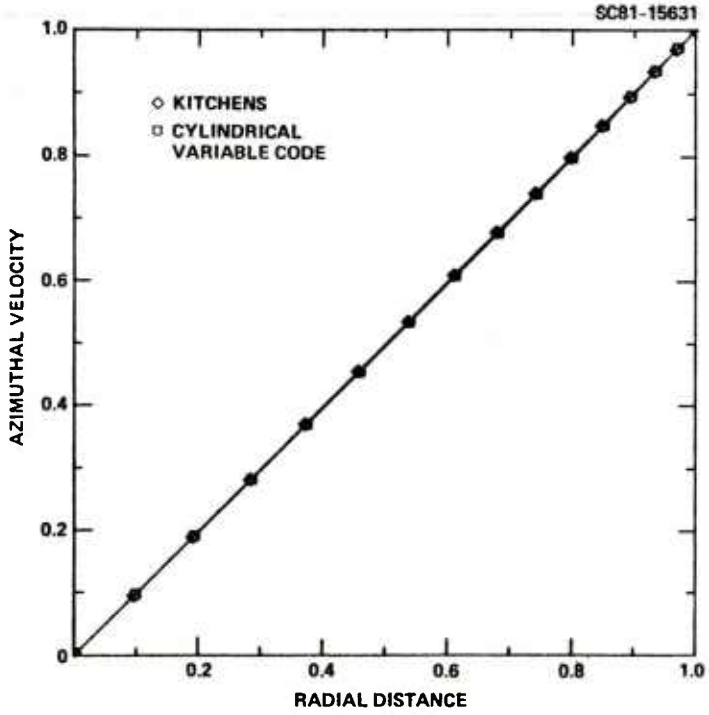

Fig. 15a. Axial location = 0.0662

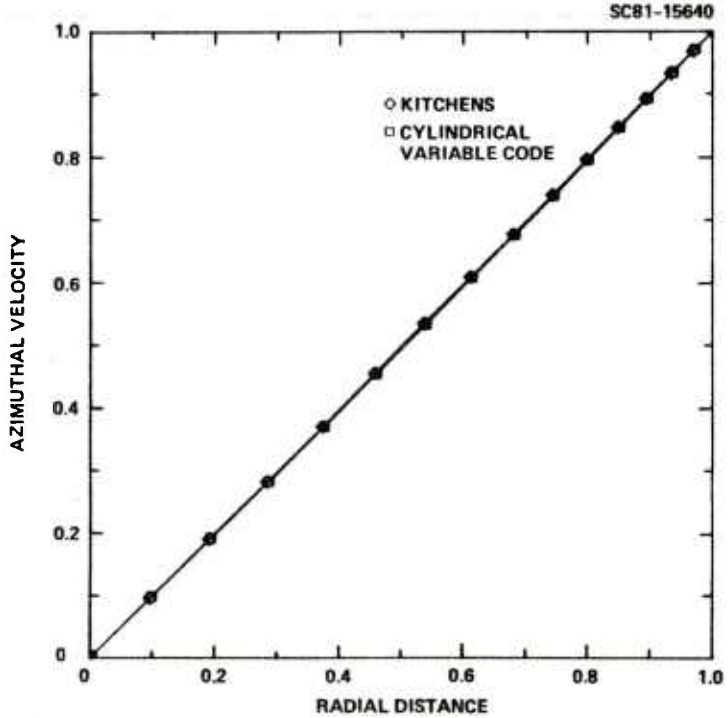

Fig. 15b. Axial location = 1.0

Fig. 15. Comparison of azimuthal velocity profiles for Reynolds number 1,000 at Time = 125.0

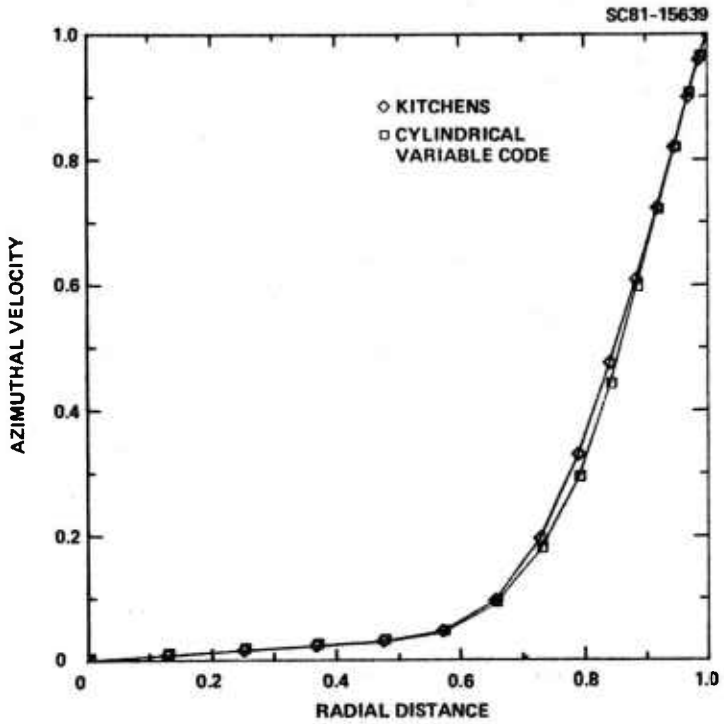

Fig. 16a. Axial location = 0.0324

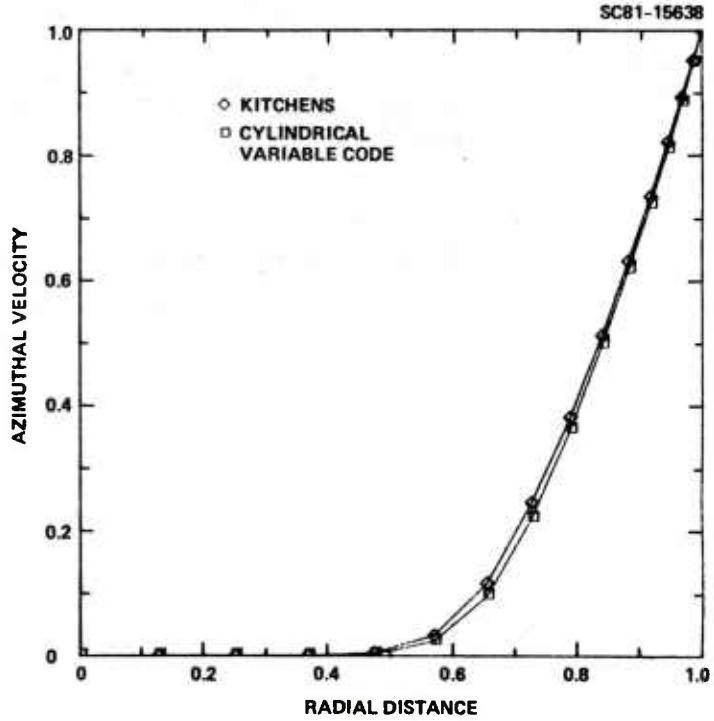

Fig. 16b. Axial location = 1.0

Fig. 16. Comparison of azimuthal velocity profiles for Reynolds number 10,000 at Time = 62.5

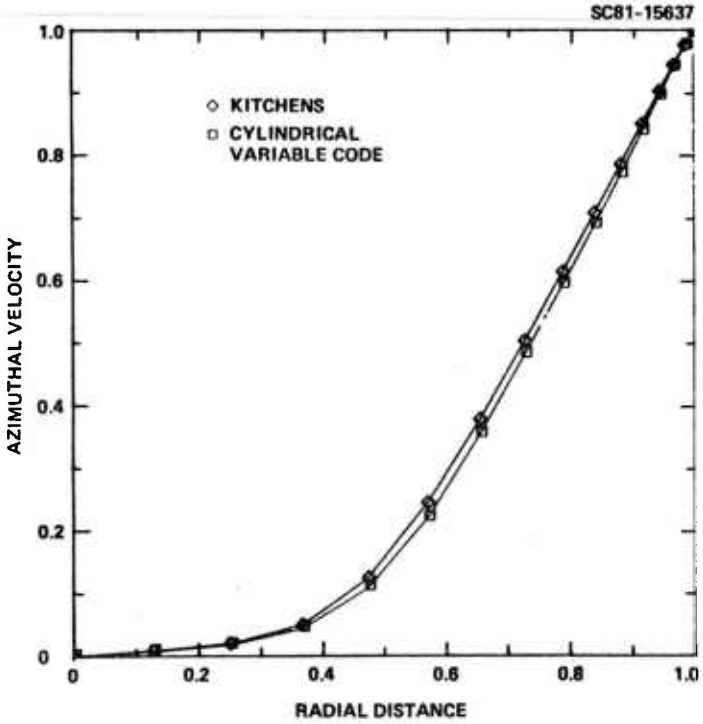

Fig. 17a. Axial location = 0.0324

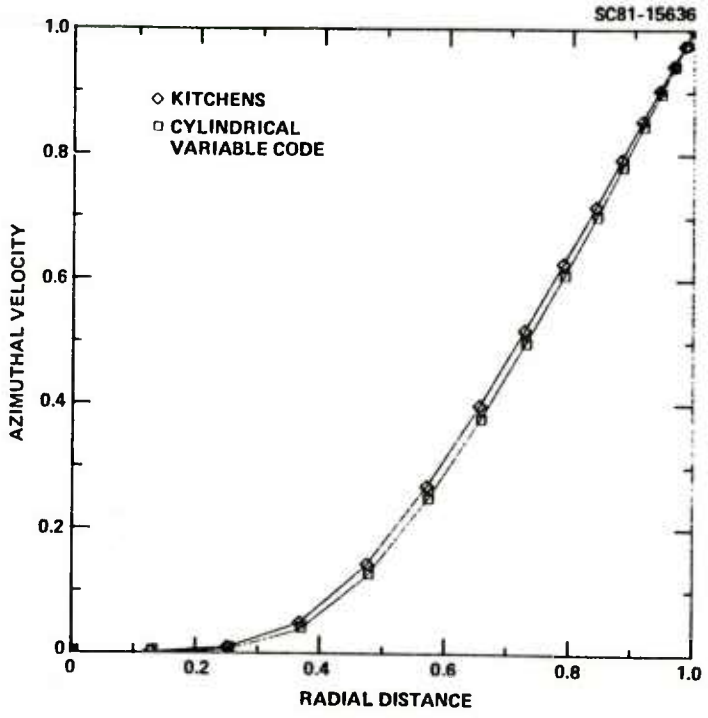

Fig. 17b. Axial location = 1.0

Fig. 17. Comparison of azimuthal velocity profiles for Reynolds number 10,000 at Time = 125.0

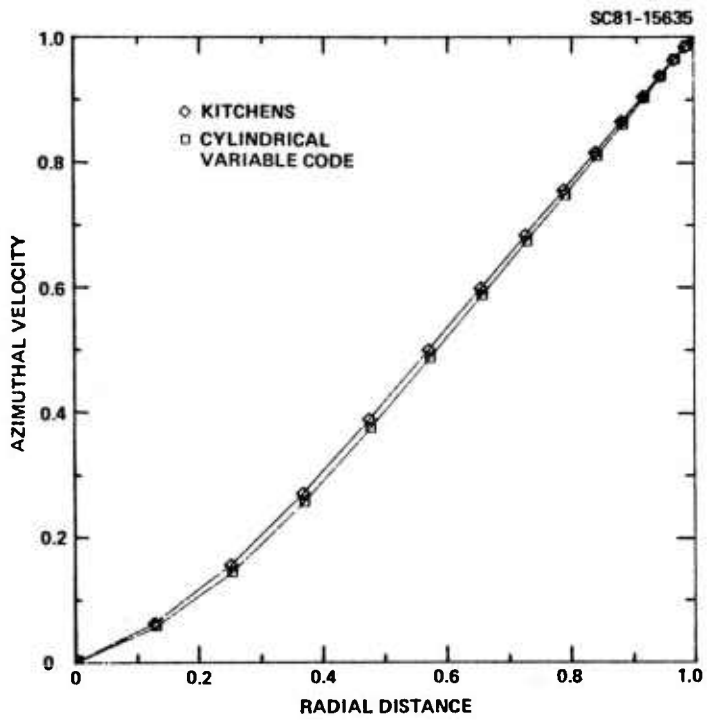

Fig. 18a. Axial location = 0.0324

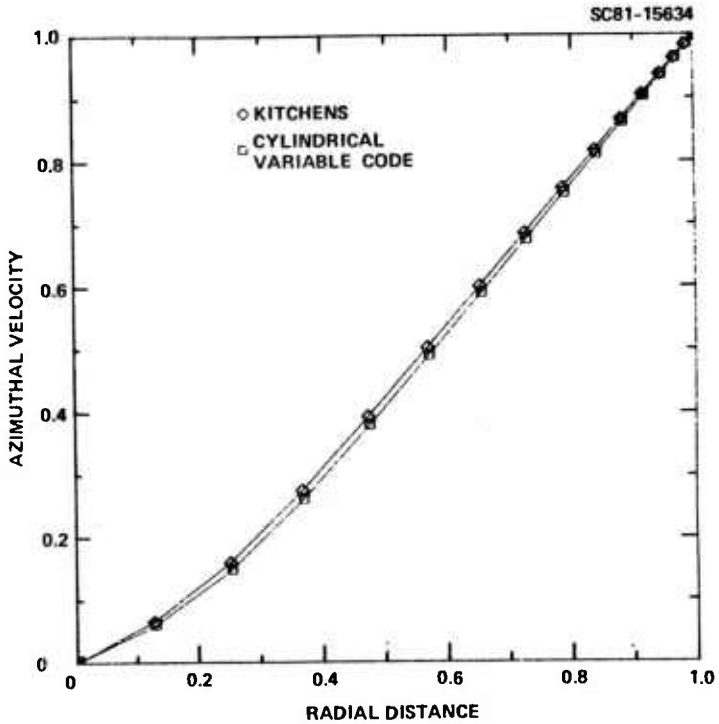

Fig. 18b. Axial location = 1.0

Fig. 18. Comparison of azimuthal velocity profiles for Reynolds number 10,000 at Time = 187.5

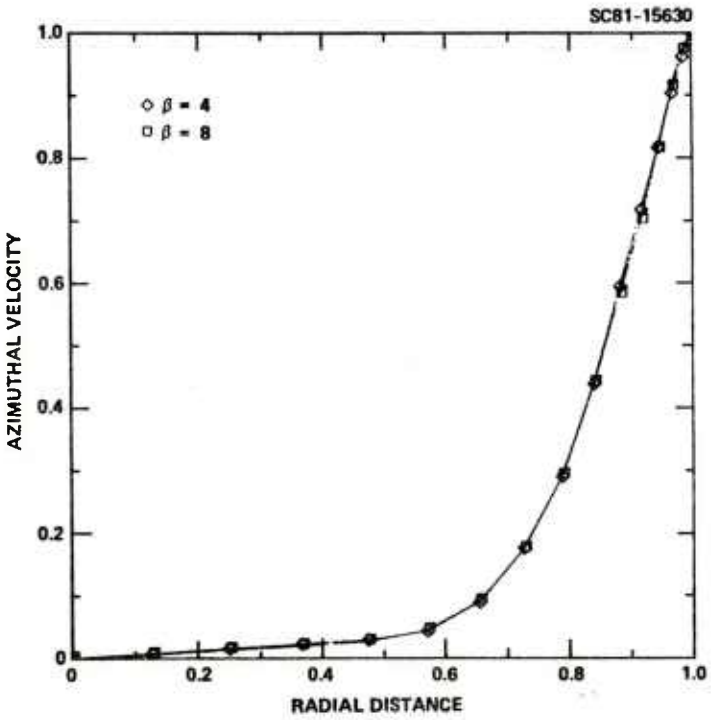

Fig. 19a. Axial location = 0.0324

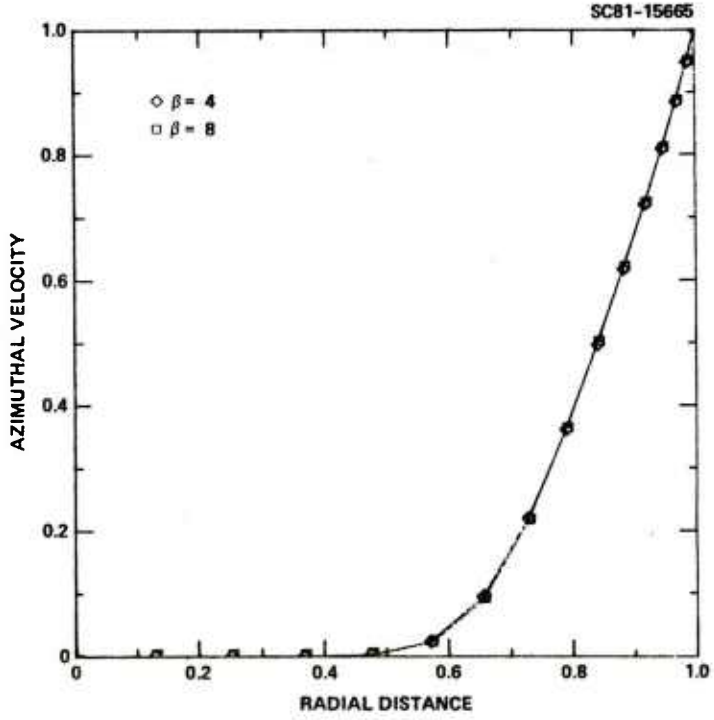

Fig. 19b. Axial location = 1.0

Fig. 19. Effect of the parameter β shown for Reynolds number 10,000 at Time = 62.5

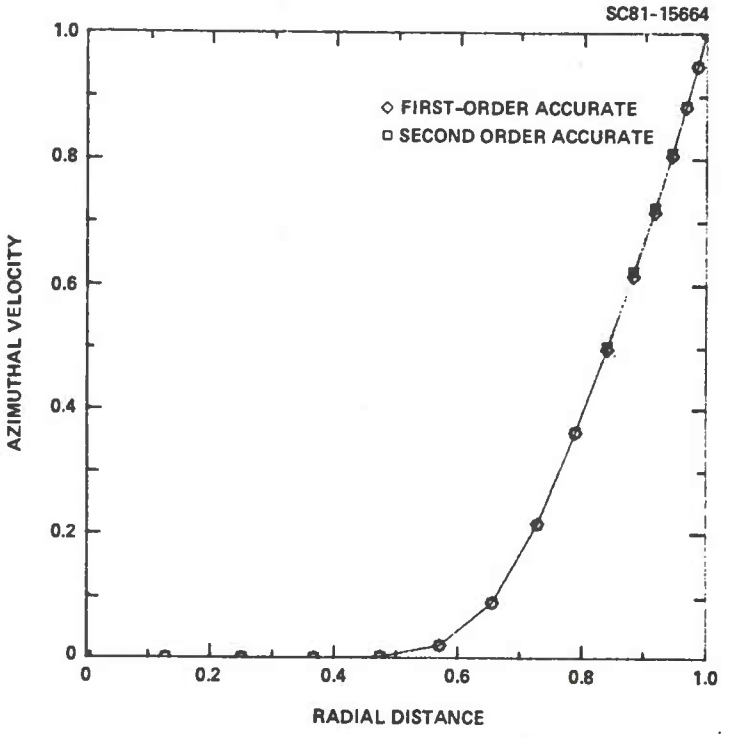

Fig. 20. Effect of time accuracy.

computational method, results were obtained for 500 steps (step size = 0.25) for a Reynolds number of a million. The computational grid for this case (41 x 41 points) is shown in Fig. 21a and azimuthal velocity profiles are shown after 250 and 500 steps in Fig. 21b. No instabilities were observed, lending credence to the prediction that the implicit scheme under consideration would not have any inherent limitations based on the magnitude of Reynolds number.

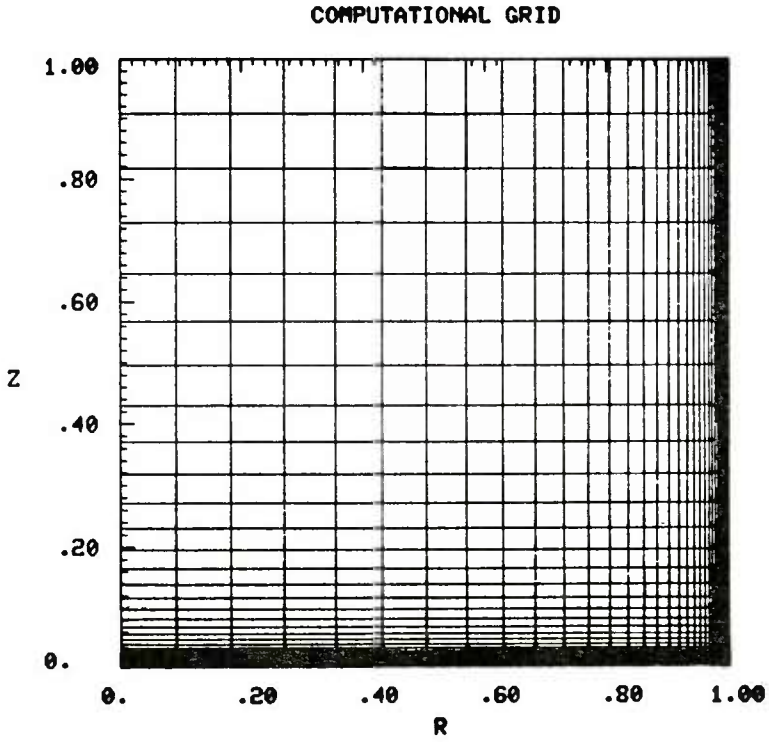

Fig. 21a. Computational grid for Reynolds number of 1,000,000.

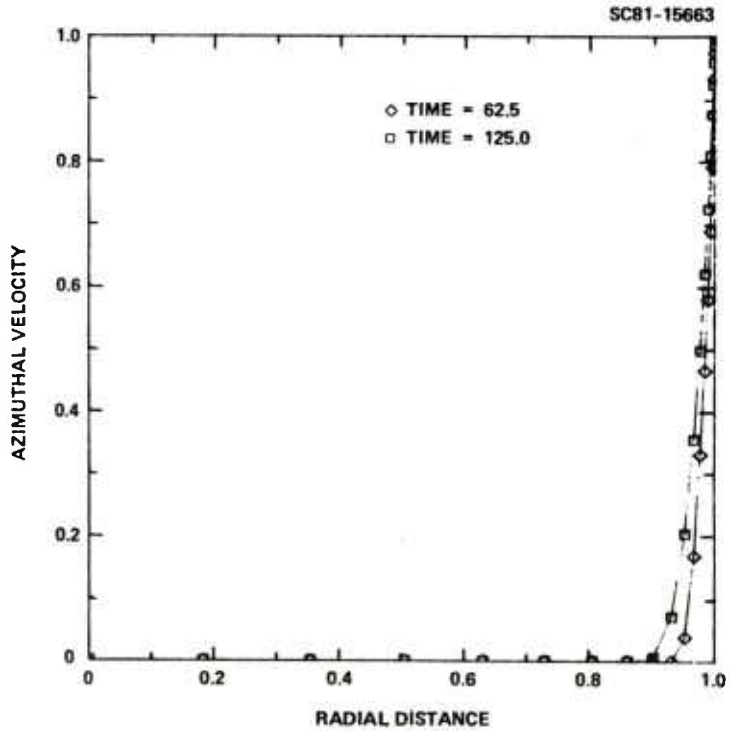

Fig. 21b. Azimuthal velocity profiles for Reynolds number of 1,000,000.

7. THREE-DIMENSIONAL RESULTS

Both the cartesian and cylindrical variable computer programs have been tested in the three-dimensional mode of operation (circumferential direction is included in the calculations), but for computing only axisymmetric flows. The axisymmetric results presented in the earlier sections could all be reproduced but at greater computational cost. No instabilities unique to the three-dimensional calculations were observed and the methods were stable for all Reynolds numbers considered (100; 1000; 10,000; 1,000,000).

A discussion of the computational speed would conclude this section. The nucleus or primary building block which must be known to compute computational time for any particular case is the time for one grid point for one iteration to be denoted by α. For the computer programs under consideration, $\alpha \simeq 0.00018$. Knowing α and the number of times this unit is repeated in a calculation, the total time required may be computed. For implicit, approximately factored schemes, the calculations are broken up into the solution of one-dimensional block tridiagonal (4 X 4 blocks) system of linear algebraic equations. Considering for example, each line of points along which only the index J varies, the time for one inversion would be proportional to JMAX, the total number of J points. There would be KMAX * LMAX such lines to be treated in the first factor of the approximate factorization. Thus, for calculating each factored segment (see Eq. 17) in the implicit method, the computational time would be proportional to the total number of points (= JMAX*KMAX*LMAX). The next point to remember is that periodic block tridiagonal inversions take about 1.7 times longer than non-periodic inversions. Thus the circumferential direction will be proportionately more expensive. Now, neglecting the time involved in computing the right hand side of Eq. (17) in comparison with the block tridiagonal inversion process, the formula that can be used to calculate an approximate

computational time for any case is given by

$$T \simeq (JMAX * KMAX * LMAX) * (2 + I_K * 1.7) * \text{NUMBER OF } \beta \text{ ITERATIONS} * \alpha \qquad (23)$$

where

T = total computational time (CPU time)

α = CPU time for 1 grid point for 1 iteration $\simeq$ 0.00018 (for CDC 7600)

I_K = 0 for two-dimensional calculations (no circumferential direction included in calculations)

= 1 for three-dimensional calculations (circumferential direction included in calculations with periodic boundary conditions)

Thus for example, a two-dimensional calculation for 250 time steps with a grid of 31 X 31 points and two β iterations per step would take 173 CPU seconds on a CDC 7600. A 21 X 21 X 20(circumferential) grid would need 1175 CPU seconds for 100 time steps with two β iterations each step. In contrast, the code developed by Kitchens would only take 37 seconds for the first example (31 X 31 points, 250 time steps). However, the Kitchens technique, being based on an axisymmetric stream-function, cannot be directly extended to three-dimensional problems.

8. CONCLUDING REMARKS

This report describes the successful development of a numerical simulation capability for liquid filled projectiles applicable to three-dimensional flow. The emphasis, in this effort, has been on proving the method by comparison with other known results for axisymmetric flow and testing the scheme for limitations and cost when operated in the fully three-dimensional mode. In terms of the task breakdown given in Section 2 (Introduction), Tasks 1-3 have been covered in Sections 3 and 4, Tasks 4 and 6 have been discussed in Sections 5 and 6, and Tasks 5 and 7 have been dealt with in Section 7. Two formulations have been developed, one based on the cartesian variables and the other based on cylindrical variables. The cylindrical variable formulation compares better with other numerical results for axisymmetric spin-up. Both formulations have proved themselves to be viable methods to be exploited in future work to compute complex three-dimensional flows with both spin and precession.

9. REFERENCES

1. Wedemeyer, E. H., "Viscous Corrections to Stewartson's Stability Criterion," BRL Report No. 1325, June 1966. AD 489687.

2. Kitchens, C. W., Jr., Gerber, N., and Sedney, R., "Oscillations of a Liquid in a Rotating Cylinder: Part I. Solid Body Rotation," BRL Technical Report No. ARBRL-TR-02081, June 1978. ADA057759.

3. Kitchens, C. W., "Navier-Stokes Solutions for Spin-Up by a Predictor-Corrector Multiple-Iteration Method," AIAA Paper No. 79-1454.

4. D'Amico, W. P., Jr., and Rogers, T. H., "Yaw Instabilities Produced by Rapidly Rotating, Highly Viscous Liquids," AIAA Paper 81-0224.

5. Steger, J. L., and Kutler, P., "Implicit Finite-Difference Procedures for the Computation of Vortex Wakes," AIAA Journal, Vol. 15, No. 4, April 1977, pp. 581-590.

6. Steger, J. L., "A Computer Program for the Internal Flow of Spin-Stabilized, Liquid Filled Shells," FSI Report 79-03, Flow Simulations, Inc., October 1979.

7. Nietubicz, C. J., Pulliam, T. H., and Steger, J. L., "Numerical Solution of the Azimuthal-Invariant Thin-Layer Navier-Stokes Equations," AIAA Paper 79-10, January 1979.

DISTRIBUTION LIST

No. of Copies	Organization
12	Administrator Defense Technical Info Center ATTN: DTIC-DDA Cameron Station Alexandria, VA 22314
1	Commander US Army Engineer Waterways Experiment Station ATTN: R.H. Malter Vicksburg, MS 39181
1	Commander US Army Materiel Development and Readiness Command ATTN: DRCDMD-ST 5001 Eisenhower Avenue Alexandria, VA 22333
1	Commander US Army Armament Research and Development Command ATTN: DRDAR-TDC (Dr. D. Gyorog) Dover, NJ 07801
2	Commander US Army Armament Research and Development Command ATTN: DRDAR-TSS Dover, NJ 07801
1	Commander US Army Armament Research and Development Command ATTN: DRDAR-LC, Dr. J. Frasier Dover, NJ 07801
6	Commander US Army Armament Research and Development Command ATTN: DRDAR-LCA-F Mr. D. Mertz Mr. E. Falkowski Mr. A. Loeb Mr. R. Kline Mr. S. Kahn Mr. S. Wasserman Dover, NJ 07801
1	Commander US Army Armament Materiel Readiness Command ATTN: DRSAR-LEP-L, Tech Lib Rock Island, IL 61299
1	Director US Army ARRADCOM Benet Weapons Laboratory ATTN: DRDAR-LCB-TL Watervliet, NY 12189
1	Commander US Army Aviation Research and Development Command ATTN: DRDAV-E 4300 Goodfellow Blvd St. Louis, MO 63120
2	Director US Army Air Mobility Research and Development Laboratory ATTN: SAVDL-D, W.J. McCroskey Ames Research Center Moffett Field, CA 94035
1	Commander US Army Communications Research and Development Command ATTN: DRDCO-PPA-SA Fort Monmouth, NJ 07703
1	Commander US Army Electronics Research and Development Command Technical Support Activity ATTN: DELSD-L Fort Monmouth, NJ 07703
1	Commander US Army Missile Command ATTN: DRSMI-R Redstone Arsenal, AL 35898
1	Commander US Army Missile Command ATTN: DRSMI-YDL Redstone Arsenal, AL 35898

DISTRIBUTION LIST

No. of Copies	Organization
1	Commander US Army Missile Command ATTN: DRSMI-RDK, Mr. R. Deep Restone Arsenal, AL 35898
1	Commander US Army Tank Automotive Research & Development Command ATTN: DRDTA-UL Warren, MI 48090
1	Commander US Army Jefferson Proving Ground ATTN: STEJP-TD-D Madison, IN 47251
1	Commander US Army Research Office ATTN: Dr. R.E. Singleton P.O. Box 12211 Research Triangle Park, NC 27709
1	AGARD-NATO ATTN: R.H. Korkegi APO New York 09777
1	Director US Army TRADOC Systems Analysis Activity ATTN: ATAA-SL, Tech Lib White Sands Missile Range NM 88002
3	Commander Naval Air Systems Command ATTN: AIR-604 Washington, DC 20360
2	Commander David W. Taylor Naval Ship Research & Development Center ATTN: H.J. Lugt, Code 1802 S. de los Santos, Head, High Speed Aero Division Bethesda, MD 20084
1	Commander Naval Surface Weapons Center ATTN: DX-21, Lib Br Dahlgren, VA 22448
4	Commander Naval Surface Weapons Center Applied Aerodynamics Division ATTN: K.R. Enkenhus M. Ciment A.E. Winklemann W.C. Ragsdale Silver Spring, MD 20910
1	AFATL (DLDL, Dr. D.C.Daniel) Eglin AFB, FL 32542
2	AFFDL (W.L. Hankey; J.S. Shang) Wright-Patterson AFB, OH 45433
5	Director National Aeronautics and Space Administration ATTN: D.R. Chapman J. Rakich W.C. Rose B. Wick P. Kutler Ames Research Center Moffett Field, CA 94035
4	Director National Aeronautics and Space Administration ATTN: E. Price J. South J.R. Sterrett Tech Library Langley Research Center Langley Station Hampton, VA 23365
1	Director National Aeronautics and Space Administration STAD-Theoretical Aero. Branch ATTN: Dr. M. D. Salas Hampton, VA 23365

DISTRIBUTION LIST

No. of Copies	Organization
1	Director National Aeronautics and Space Administration Lewis Research Center ATTN: MS 60-3, Tech Lib 21000 Brookpark Road Cleveland, OH 44135
2	Director National Aeronautics and Space Administration Marshall Space Flight Center ATTN: A.R. Felix, Chief S&E-AERO-AE Dr. W.W. Fowlis Huntsville, AL 35812
2	Director Jet Propulsion Laboratory ATTN: L.M. Mach Tech Library 4800 Oak Grove Drive Pasadena, CA 91103
3	Arnold Research Org., Inc. ATTN: J.D. Whitfield R.K. Matthews J.C. Adams Arnold AFB, TN 37389
3	Aerospace Corporation ATTN: H. Mirels R.L. Varwig Aerophysics Lab. P.O. Box 92957 Los Angeles, CA 90009
1	AVCO Systems Division ATTN: B. Reeves 201 Lowell Street Wilmington, MA 01887
3	Boeing Commercial Airplane Company ATTN: R. A. Day, Org B-8120 P.E. Rubbert, MS 3N-19 J.D. McLean, MS-3N-19 Seattle, WA 98124
3	Calspan Corporation ATTN: A. Ritter G. Homicz W. Rae P.O. Box 400 Buffalo, NY 14225
1	General Dynamics ATTN: Research Lib 2246 P.O. Box 748 Fort Worth, TX 76101
1	General Electric Company, RESD ATTN: W. J. East 3198 Chestnut Street Philadelphia, PA 19101
2	Grumman Aerospace Corporation ATTN: R.E. Melnik L.G. Kaufman Bethpage, NY 11714
2	Lockheed-Georgia Company ATTN: B.H. Little, Jr. G.A. Pounds Dept 72074, Zone 403 86 South Cobb Drive Marietta, GA 30062
1	Lockheed Missiles and Space Company ATTN: Tech Info Center 3251 Hanover Street Palo Alto, CA 94304
3	Martin-Marietta Laboratories ATTN: S.H. Maslen S.C. Traugott H. Obremski 1450 S. Rolling Road Baltimore, MD 21227
2	McDonnell Douglas Astronautics Corporation ATTN: J. Xerikos H. Tang 5301 Bolsa Avenue Huntington Beach, CA 92647

DISTRIBUTION LIST

No. of Copies	Organization
2	McDonnell-Douglas Corporation Douglas Aircraft Company ATTN: T. Cebeci K. Stewartson 3855 Lakewood Boulevard Long Beach, CA 90801
2	Rockwell International Science Center ATTN: Dr. V. Shankar Dr. N. Malmuth 1049 Camino Dos Rios Thousand Oaks, CA 91360
2	Sandia Laboratories ATTN: F.G. Blottner Tech Lib. Albuquerque, NM 87115
1	Union Carbide Nuclear Division ATTN: Dr. J.E. Park, MS 53 Bldg. K-1007 P.O. Box P Oak Ridge, TN 37830
2	United Aircraft Corporation Research Laboratories ATTN: M.J. Werle Library East Hartford, CT 06108
1	LVT Aerospace Corp. Vought Systems Division ATTN: J.M. Cooksey, Chief, Gas Dynamics Lab, 2-53700 P.O. Box 5907 Dallas, TX 75222
1	Arizona State University Department of Mechanical and Energy Systems Engineering ATTN: G.P. Neitzel Tempe, AZ 85281
3	California Institute of Technology ATTN: Tech Library H.B. Keller Mathematics Dept. D. Coles Aeronautics Dept. Pasadena, CA 91102
1	Cornell University Graduate School of Aero Engr ATTN: Library Ithaca, NY 14850
1	Illinois Institute of Tech H. M. Nagib 3300 South Federal Chicago, IL 60616
1	The Johns Hopkins University Department of Mechanics and Materials Science ATTN: S. Corrsin Baltimore, MD 21218
4	The Johns Hopkins University Applied Physics Laboratory ATTN: Dr. R.D. Whiting Dr. D.A. Hurdif Dr. R.S. Hirsh Mr. E.R. Bohn Johns Hopkins Road Laurel, MD 20707
1	University of California Lawrence Livermore National Laboratory ATTN: Dr. Viecelli Livermore, CA 94550
3	Massachusetts Institute of Technology ATTN: E. Covert H. Greenspan Tech Lib 77 Massachusetts Avenue Cambridge, MA 02139

DISTRIBUTION LIST

No. of Copies	Organization
2	North Carolina State Univ Mechanical and Aerospace Engineering Department ATTN: F.F. DeJarnette J.C. Williams Raleigh, NC 27607
1	Notre Dame University Department of Aero Engr ATTN: T.J. Mueller South Bend, IN 46556
2	Ohio State University Dept of Aeronautical and Astronautical Engineering ATTN: S.L. Petrie O.R. Burggraf Columbus, OH 43210
2	Polytechic Institute of New York ATTN: G. Moretti S.G. Rubin Route 110 Farmingdale, NY 11735
3	Princeton University James Forrestal Research Ctr Gas Dynamics Laboratory ATTN: S.M. Bogdonoff S.I. Cheng Tech Library Princeton, NJ 08540
1	Purdue University Thermal Science & Prop Ctr ATTN: Tech Library W. Lafayette, IN 47907
1	Rensselaer Polytechnic Institute Department of Math Sciences ATTN: R.C. Diprima Troy, NY 12181
1	San Diego State University Department of Aerospace Engr and Engineering Mechanics College of Engineering ATTN: K.C. Wang San Diego, CA 92182
1	Southern Methodist University Department of Civil and Mechanical Engineering ATTN: R.L. Simpson Dallas, TX 75275
1	Southwest Research Institute Applied Mechanics Reviews 8500 Culebra Road San Antonio, TX 78228
6	Stanford University Dept of Aeronautics/Astronautics ATTN: Dr. J.L. Steger (3 cys) Dr. S. Chakravarthy (3 cys) Stanford, CA 94305
1	Texas A&M University College of Engineering ATTN: R.H. Page College Station, TX 77843
1	University of California - Berkeley Department of Aerospace Engineering ATTN: M. Holt Berkeley, CA 94720
1	University of California - Davis ATTN: H.A. Dwyer Davis, CA 95616

DISTRIBUTION LIST

No. of Copies	Organization
2	University of California - San Diego Department of Aerospace Engineering and Mechanical Engineering Sciences ATTN: P. Libby Tech Library La Jolla, CA 92037
1	University of Cincinnati Department of Aerospace Engineering ATTN: R.T. Davis Cincinnati, OH 45221
1	University of Colorado Department of Astro-Geophysics ATTN: E.R. Benton Boulder, CO 80302
1	University of Hawaii Dept of Ocean Engineering ATTN: G. Venezian Honolulu, HI 96822
2	University of Maryland ATTN: W. Melnik J.D. Anderson College Park, MD 20742
2	University of Michigan Department of Aeronautical Engineering ATTN: W.W. Wilmarth Tech Library East Engineering Building Ann Arbor, MI 48104
1	University of Santa Clara Department of Physics ATTN: R. Greeley Santa Clara, CA 95053
3	University of Southern California Department of Aerospace Engineering ATTN: T. Maxworthy P. Weidman L.G. Redekopp Los Angeles, CA 90007
1	University of Texas Department of Aerospace Engineering ATTN: J.C. Westkaemper Austin, TX 78712
1	University of Virginia Department of Aerospace Engineering & Engineering Physics ATTN: I.D. Jacobson Charlottesville, VA 22904
1	University of Virginia Research Laboratories for the Engineering Sciences ATTN: Prof. H. G. Wood P.O. Box 3366 University Station Charlottesville, VA 22903
1	University of Washington Department of Mechanical Engineering ATTN: Tech Library Seattle, WA 98105
1	University of Wyoming ATTN: D.L. Boyer University Station Laramie, WY 82071
1	Virginia Polytechnic Institute and State University Department of Aerospace Engineering ATTN: Tech Library Blacksburg, VA 24061

DISTRIBUTION LIST

No. of Copies	Organization
1	Woods Hole Oceanographic Institute ATTN: J.A. Whitehead Woods Hole, MA 02543

Aberdeen Proving Ground

Director, USAMSAA
ATTN: DRXSY-D
DRXSY-MP, H. Cohen

Commander, USATECOM
ATTN: DRSTE-TO-F

Director, USACSL, Bldg. E3330, EA
ATTN: Munitions Division
W.C. Dee

Director, USACSL, Bldg. E3516, EA
ATTN: DRDAR-CLB-PA

USER EVALUATION OF REPORT

Please take a few minutes to answer the questions below; tear out this sheet, fold as indicated, staple or tape closed, and place in the mail. Your comments will provide us with information for improving future reports.

1. BRL Report Number _____

2. Does this report satisfy a need? (Comment on purpose, related project, or other area of interest for which report will be used.)

_____

_____

_____

3. How, specifically, is the report being used? (Information source, design data or procedure, management procedure, source of ideas, etc.) _____

_____

_____

4. Has the information in this report led to any quantitative savings as far as man-hours/contract dollars saved, operating costs avoided, efficiencies achieved, etc.? If so, please elaborate.

_____

_____

5. General Comments (Indicate what you think should be changed to make this report and future reports of this type more responsive to your needs, more usable, improve readability, etc.) _____

_____

_____

_____

6. If you would like to be contacted by the personnel who prepared this report to raise specific questions or discuss the topic, please fill in the following information.

Name: _____

Telephone Number: _____

Organization Address: _____

_____

_____